Physical Chemistry Chemical Physics

c8cp04173c

We have presented the Graphical Abstract text and image for your article below. This brief summary of your work will appear in the contents pages of the issue in which your article appears.

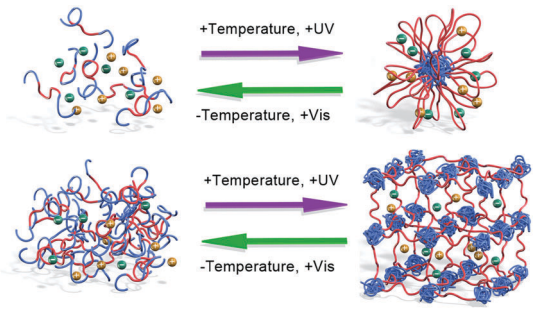

Block copolymer self-assembly in ionic liquids

Ryota Tamate, Kei Hashimoto, Takeshi Ueki and Masayoshi Watanabe*

Recent developments in block copolymer self-assembly in ionic liquids are reviewed from both fundamental and applied aspects.

Q2

Please check this proof carefully. Our staff will not read it in detail after you have returned it.

Please send your corrections either as a copy of the proof PDF with electronic notes attached or as a list of corrections. **Do not edit the text within the PDF or send a revised manuscript** as we will not be able to apply your corrections. Corrections at this stage should be minor and not involve extensive changes.

Proof corrections must be returned as a single set of corrections, approved by all co-authors. No further corrections can be made after you have submitted your proof corrections as we will publish your article online as soon as possible after they are received.

Please ensure that:

- The spelling and format of all author names and affiliations are checked carefully. You can check how we have identified the authors' first and last names in the researcher information table on the next page. **Names will be indexed and cited as shown on the proof, so these must be correct.**
- Any funding bodies have been acknowledged appropriately and included both in the paper and in the funder information table on the next page.
- All of the editor's queries are answered.
- Any necessary attachments, such as updated images or ESI files, are provided.

Translation errors can occur during conversion to typesetting systems so you need to read the whole proof. In particular please check tables, equations, numerical data, figures and graphics, and references carefully.

Please return your **final** corrections, where possible within **48 hours** of receipt, by e-mail to: pccp@rsc.org. If you require more time, please notify us by email.

Funding information

Providing accurate funding information will enable us to help you comply with your funders' reporting mandates. Clear acknowledgement of funder support is an important consideration in funding evaluation and can increase your chances of securing funding in the future.

We work closely with Crossref to make your research discoverable through the Funding Data search tool (http://search.crossref.org/funding). Funding Data provides a reliable way to track the impact of the work that funders support. Accurate funder information will also help us (i) identify articles that are mandated to be deposited in **PubMed Central (PMC)** and deposit these on your behalf, and (ii) identify articles funded as part of the **CHORUS** initiative and display the Accepted Manuscript on our web site after an embargo period of 12 months.

Further information can be found on our webpage (http://rsc.li/funding-info).

What we do with funding information

We have combined the information you gave us on submission with the information in your acknowledgements. This will help ensure the funding information is as complete as possible and matches funders listed in the Crossref Funder Registry.

If a funding organisation you included in your acknowledgements or on submission of your article is not currently listed in the registry it will not appear in the table on this page. We can only deposit data if funders are already listed in the Crossref Funder Registry, but we will pass all funding information on to Crossref so that additional funders can be included in future.

Please check your funding information

The table below contains the information we will share with Crossref so that your article can be found *via* the Funding Data search tool. **Please check that the funder names and grant numbers in the table are correct and indicate if any changes are necessary to the Acknowledgements text.**

Funder name	Funder's main country of origin	Funder ID (for RSC use only)	Award/grant number
Japan Society for the Promotion of Science	Japan	501100001691	15H05758, 17J00756, 18K14280, 25000003

Q1

Researcher information

Please check that the researcher information in the table below is correct, including the spelling and formatting of all author names, and that the authors' first, middle and last names have been correctly identified. **Names will be indexed and cited as shown on the proof, so these must be correct.**

If any authors have ORCID or ResearcherID details that are not listed below, please provide these with your proof corrections. Please ensure that the ORCID and ResearcherID details listed below have been assigned to the correct author. Authors should have their own unique ORCID iD and should not use another researcher's, as errors will delay publication.

Please also update your account on our online manuscript submission system to add your ORCID details, which will then be automatically included in all future submissions. See here for step-by-step instructions and more information on author identifiers.

First (given) and middle name(s)	Last (family) name(s)	ResearcherID	ORCID iD
Ryota	Tamate		0000-0002-1704-1058
Kei	Hashimoto		
Takeshi	Ueki		0000-0001-9317-6280
Masayoshi	Watanabe	M-4816-2014	0000-0003-4092-6150

Queries for the attention of the authors

Journal: **PCCP**

Paper: **c8cp04173c**

Title: **Block copolymer self-assembly in ionic liquids**

For your information: You can cite this article before you receive notification of the page numbers by using the following format: (authors), Phys. Chem. Chem. Phys., (year), DOI: 10.1039/c8cp04173c.

Editor's queries are marked on your proof like this Q1, Q2, etc. and for your convenience line numbers are indicated like this 5, 10, 15, ...

Please ensure that all queries are answered when returning your proof corrections so that publication of your article is not delayed.

Query reference	Query	Remarks
Q1	The award/grant numbers in the article text and in the funder information do not match, please check and correct as necessary.	
Q2	Please confirm that the spelling and format of all author names is correct. Names will be indexed and cited as shown on the proof, so these must be correct. No late corrections can be made.	

PCCP

PERSPECTIVE

Block copolymer self-assembly in ionic liquids

Cite this: DOI: 10.1039/c8cp04173c

Ryota Tamate, †[a] Kei Hashimoto,†[a] Takeshi Ueki [b] and Masayoshi Watanabe *[a]

Received 2nd July 2018,
Accepted 6th August 2018

DOI: 10.1039/c8cp04173c

rsc.li/pccp

Ionic liquids (ILs), solely composed of cations and anions, are regarded as a novel class of promising liquids, potentially applicable to energy devices, reaction media, separation materials, *etc.* ILs have also attracted great attention as new media for molecular self-assembly, capable of producing novel soft materials with unique features never observed for conventional soft materials containing organic and aqueous solvents. In this review, we focus on recent developments in block copolymer (BCP) self-assembly in ILs. Self-assembled structures formed by dilute and concentrated BCP solutions in ILs are discussed in detail. Ion gels formed by BCP self-assembly have received special interest because they exhibit excellent physical properties of tunable viscoelasticity and solution processability without impairing the intrinsic properties of ILs, such as nonvolatility, nonflammability, and high ionic conductivity. Applications of ion gels based on BCP self-assembly for electric double layer capacitors, lithium-ion batteries, and electroactive soft actuators are also addressed.

1. Introduction

Block copolymers (BCPs), defined as polymers composed of blocks of chemically distinct repeat units, are classified by the number of monomer types and the sequences; for example, the simplest sequence, obtained by two-step polymerization of A and B monomers, is the AB-type diblock copolymer, whereas two-step polymerization from a bifunctional initiator or three-step polymerization gives ABA-type or BAB-type triblock

[a] *Department of Chemistry and Biotechnology, Yokohama National University, 79-5 Tokiwadai, Hodogaya-ku, Yokohama 240-8501, Japan. E-mail: mwatanab@ynu.ac.jp; Fax: +81-45-339-3955; Tel: +81-45-339-3955*

[b] *WPI Research Center International Center for Materials Nanoarchitectonics (WPI-MANA), National Institute for Materials Science (NIMS), 1-1 Namiki, Tsukuba, Ibaraki, 305-0044, Japan*

† These authors contributed equally to this work.

Ryota Tamate

Ryota Tamate received his BS (2006) and MS (2008) degrees from Kyoto University. After working at Bridgestone Co. (2008–2013), he received a PhD degree in 2016 from the University of Tokyo under the supervision of Professor Ryo Yoshida. He was a recipient of a JSPS Fellowship for Young Scientists (2014–2017). In 2017, he earned President's and Dean's Awards from the University of Tokyo. He is currently working as a JSPS Postdoctoral Fellow with Professor Masayoshi Watanabe at Yokohama National University. His research interests include block copolymer self-assembly, polymers in ionic liquids and functional soft materials.

Kei Hashimoto

Kei Hashimoto was born in 1989 in Yokohama. He received his MS (2013) and PhD degrees (2016) from the University of Tokyo under the supervision of Prof. Mitsuhiro Shibayama. He was awarded with the Research Fellowship for Young Scientists from the JSPS (2015–2016). He is currently working as research fellow at Yokohama National University with Prof. Masayoshi Watanabe. His research mainly focuses on solution chemistry of ionic liquids, light scattering analysis for soft material, and microscopic structures of ionic liquids and ion gels.

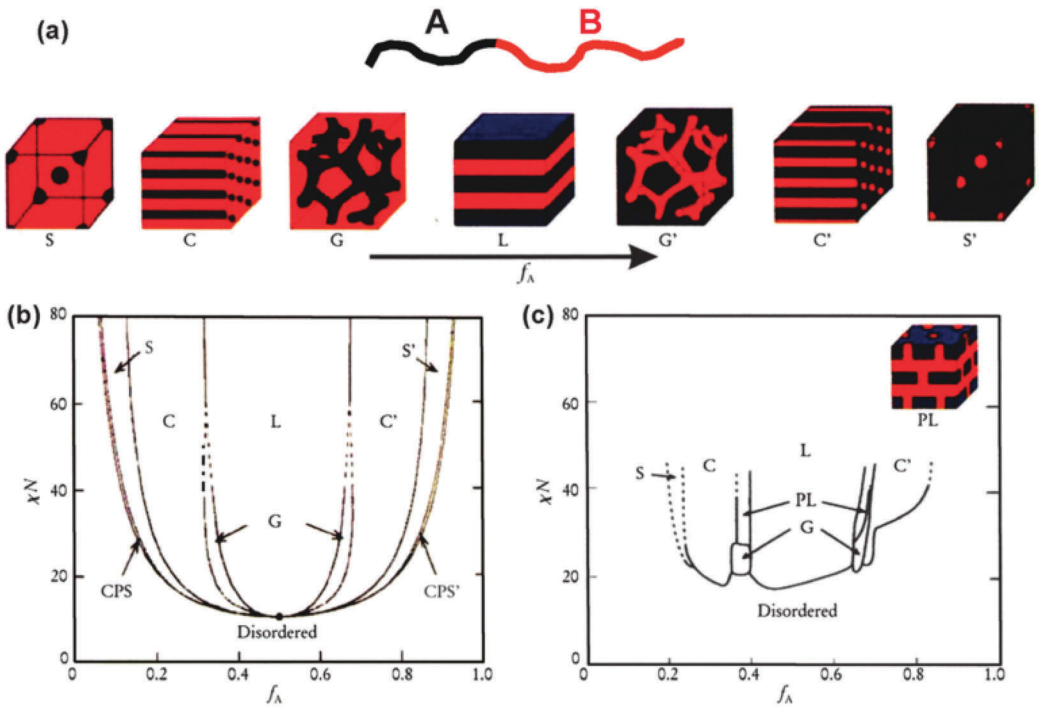

Fig. 1 (a) Representative illustrations of microphase-separated structures: spherical (S), cylindrical (C), gyroid (G), and lamellar (L) structures. Phase diagrams for AB-type diblock copolymers obtained from (b) the self-consistent mean-field theory and (c) experiments with polyisoprene-*b*-polystyrene (PI-*b*-PS) diblock copolymers. The morphologies depend on the volume fraction of the A monomer (f_A) and χN, where χ is the Flory–Huggins interaction parameter and N is the degree of polymerization. CPS and PL correspond to close-packed spheres and perforated layers, respectively. Reproduced with permission from ref. 32. The Royal Society of Chemistry 2012.

copolymers. If they are amphiphilic, BCPs in melts spontaneously separate into two phases to minimize the Gibbs free energy of mixing. This phenomenon is mainly explained by the Flory–Huggins model, based on the interaction energies between A and B monomers and the entropy of the arrangement of polymer chains:[1]

$$\Delta G_{\mathrm{mix}} = \Delta H_{\mathrm{mix}} - T\Delta S_{\mathrm{mix}} = kT\left[\chi f_{\mathrm{A}}(1-f_{\mathrm{A}}) + \frac{f_{\mathrm{A}}}{N_{\mathrm{A}}}\ln f_{\mathrm{A}} + \frac{1-f_{\mathrm{A}}}{N_{\mathrm{B}}}\ln(1-f_{\mathrm{A}})\right]$$

Takeshi Ueki

Takeshi Ueki earned his PhD degree at Yokohama National University (2007) under the supervision of Professor Masayoshi Watanabe. He worked postdoctoral associate at University of Minnesota (2007–2008), at Yokohama National University (2008–2011), and at University of Tokyo as JSPS research fellow, SPD (2011-2013). He is currently working at National Institute for Materials Science (NIMS) as senior researcher and at Hokkaido University as visiting associate professor. He received the award for encouragement of research in polymer science from SPSJ (2011). His research interest includes stimuli-responsive (block co)polymers, gels, and chemical oscillation reaction in protic ionic liquids.

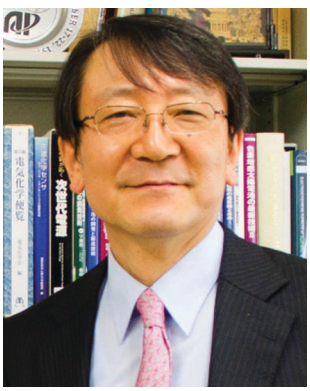

Masayoshi Watanabe

Masayoshi Watanabe is a Professor of Yokohama National University. He received his BS, MS, and PhD degrees from Waseda University. He joined Sophia University in 1982 as an Assistant Professor. In 1992, he moved to Yokohama National University and was promoted to full Professor in 1998. He received the Award of the Society of Polymer Science, Japan in 2006, and the Award of The Electrochemical Society of Japan (Takei Award) and ECS Max Bredig Award in 2016. His current research interests include the design of ionic liquids and polymers for electrochemical applications and the phase-behavior and self-assembly of polymers in ionic liquids.

where ΔG_{mix}, ΔH_{mix}, and ΔS_{mix} are the Gibbs free energy, enthalpy, and entropy of mixing, respectively, T is the absolute temperature, k is the Boltzmann constant, f_A is the volume fraction of the A monomer, N_A and N_B are the polymerization degrees of the A and B monomers, respectively, and χ is the enthalpic interaction parameter between the A and B monomers (χ parameter; higher χ promotes phase separation).

In BCP systems, the covalent bonds between two blocks prevent macroscopic phase separation, instead forcing BCPs to form a variety of microphase-separated structures.[2,3] Fig. 1a shows the microphase-separated structures in AB-type diblock copolymer melts. With increasing f_A, the microphase-separated structure undergoes morphological transitions from disordered to spherical (S), cylindrical (C), gyroid (G), lamellar (L), and their reverse structures. These morphologies were theoretically predicted by Leibler[2] and by Bates, Fredrickson, Matsen, *et al.*[3–7] and experimentally confirmed by Bates and co-workers.[3,4,8] Fig. 1b shows a phase diagram for AB-type diblock copolymer melts calculated from the self-consistent mean-field theory.[5] The microphase-separated structures observed in this system depend on f_A and χN. At high χN, disordered, spherical (S), cylindrical (C), and lamellar (L) structures were predicted, whereas gyroid (G) structures, which are composed of bicontinuous A and B phases,[9] additionally appear at low χN. In both cases, close-packed spheres (CPS) were predicted to be observed in a narrow region. The formation of these structures was confirmed by transmission electron microscopy (TEM) of polyisoprene-*b*-polystyrene (PI-*b*-PS) membranes with varying compositions at various temperatures (Fig. 1c).[8] The obtained phase diagram is very similar to the theoretical one (Fig. 1b), with some exceptions (*i.e.*, the asymmetric shape of the diagram and the metastable perforated layers (PL)[10]), indicating that f_A and χN are reasonable parameters for controlling microphase-separated structures.

During the development of microstructural investigations of BCPs, it is noteworthy that advances in the living polymerization of BCPs enabled control of the degree of polymerization, N, of the polymers with a narrow molecular weight distribution. Furthermore, living radical polymerizations, including atom transfer radical polymerization (ATRP) established by Sawamoto, Matyjaszewski, *et al.*[11–16] and reversible addition–fragmentation chain transfer polymerization (RAFT) established by Thang and co-workers,[17,18] greatly contributed to the broad range of options for monomers and sequences, such as ABA-type and ABC-type triblock,[18–20] grafted,[21] star-shaped,[22] and hyperbranched copolymers.[23] Generally, BCPs containing two monomer components (ABA-type or BAB-type BCPs) show analogous phase diagrams to those of AB-type diblock copolymers.[24,25] However, the addition of a third component, as typified by ABC-type BCPs, results in more sophisticated microphase-separated structures, completely different from those observed in the diblock system.[3,26–28] Similarly, the addition of solvent to a BCP system results in complicated morphological changes.[29–33] In dilute BCP solutions, amphiphilic BCPs self-assemble into micelles with a solvatophobic core and a solvatophilic corona, analogous to surfactants.[34]

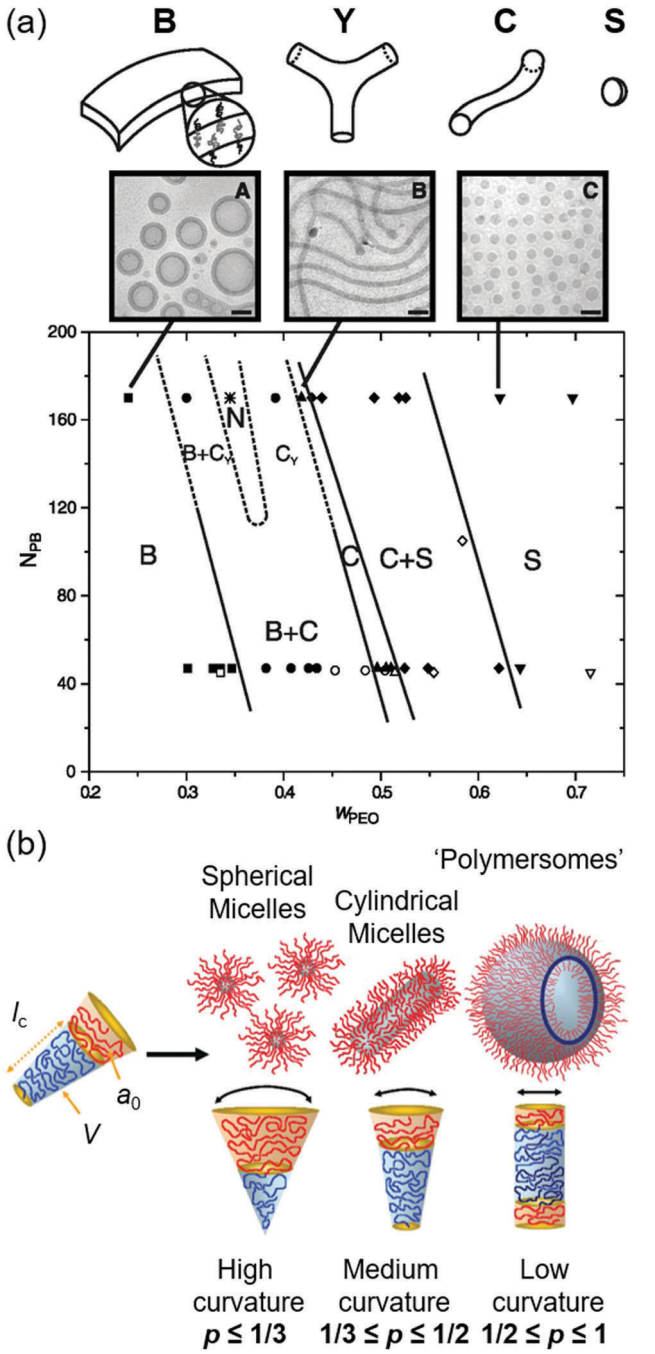

Fig. 2 (a) Morphology diagram for poly(1,2-butadiene)-*b*-poly(ethylene oxide) (PB-*b*-PEO) in water (polymer concentration: 1 wt%) as a function of the degree of polymerization of the PB block (N_{PB}) and the weight fraction of the PEO block (w_{PEO}). The morphologies (bilayer vesicles (B), cylindrical micelles (C), spherical micelles (S), and three-dimensional networks (N)), identified by cryo-TEM, are illustrated above the graph. C$_Y$ corresponds to a cylinder connected by Y-junctions. The scale bars (in A–C) are 100 nm. Reproduced with permission from ref. 35. American Association for the Advancement of Science 2003. (b) Schematic models of the morphologies of BCPs in a block-selective solvent. The dimensionless packing parameter, p, calculated from the curvature of the molecules is a key factor for the formation of the microstructures. Reproduced with permission from ref. 38. Wiley 2009.

Fig. 2a shows typical morphologies and the phase diagram observed in the binary mixture of water and poly(1,2-

butadiene)-*b*-poly(ethylene oxide) (PB-*b*-PEO) diblock copolymer.[35] The BCP mainly forms spherical micelles (S), cylindrical micelles (C), and bilayer vesicles (B), and the phases containing two morphologies, which depend on the degree of polymerization of the PB block (N_{PB}) and the weight fraction of the PEO block (w_{PEO}). In such a mixture, the selectivity of the solvent (*i.e.*, the solubility of the A and B blocks in the solvent) plays a key role, as does the volume fraction of the solvent.[36,37] In a selective solvent, the curvature of the interface between the A and B blocks changes owing to selective swelling of the block (Fig. 2b). The curvature of BCP can be evaluated using the packing parameter, $p = v/(a_0 l_c)$, where v is the volume of the solvatophobic chain, a_0 is the optimal area of the solvatophilic chain, and l_c is the length of the solvatophobic chain. Generally, BCPs form spherical micelles at $p < 1/3$, cylindrical micelles at $1/3 < p < 1/2$, and polymersomes (or bilayer vesicles) at $p > 1/2$.[38] From this viewpoint, it is reasonable that a decrease in w_{PEO} strongly affects the morphologies, resulting in the transition from spherical micelles to vesicles in Fig. 2a. Although these complexities of self-assembly increase the difficulty of predicting the microstructures, they also provide the opportunity to change the size and morphology of the microstructure considerably by changing the volume fraction of the blocks or solvent. In other words, the self-assembled structures of BCPs can be controlled by tuning the amount of a single component, providing a versatile method for fabricating ordered microstructures.

2. Ionic liquids as solvents for polymers

The melting temperatures of salts strongly depend on the Lewis acidity of the cations and the Lewis basicity of the anions (Fig. 3).[39] The combination of anions and cations with weak Lewis acidity and basicity forms salts with low melting temperatures, *i.e.*, room-temperature ionic liquids (ILs). ILs, composed entirely of ions, exhibit unique properties such as thermal and electrochemical stability, negligible volatility, non-flammability, and high ionic conductivity.[39–42]

ILs are generally regarded as novel green solvents,[43] applicable to the extraction, partition, and separation of various target molecules, and as electrolytes for electrochemical devices.[44,45] The properties of ILs can be designed by the combination of cations and anions, which enables tuning of the properties, including hydrophilicity and hydrophobicity, Lewis acidity and basicity, and hydrogen bonding ability. From this viewpoint, ILs can often be used as solvents for biopolymers[46–50] and catalytic reactions.[51] ILs also exhibit good compatibility with various synthetic polymers, allowing the preparation of functional soft materials.[52,53] Stimuli-responsive phase separation is one of the interesting properties of mixtures of ILs and polymers.[54] Poly(*N*-isopropylacrylamide) (PNIPAm) is a well-known thermoresponsive polymer that exhibits lower critical solution temperature (LCST)-type phase separation in aqueous solutions at ambient temperature. At low temperatures, PNIPAm is soluble in water and forms homogeneous solutions, whereas it is insoluble at high temperatures and forms turbid solutions.[55] In contrast, PNIPAm exhibits upper critical solution temperature (UCST)-type phase separation in imidazolium-based ILs ($[C_n\text{mim}][NTf_2]$) at ambient temperature (Fig. 4a).[56] From the viewpoint of thermodynamics, the mixing Gibbs energy, $\Delta G_{mix} = \Delta H_{mix} - T\Delta S_{mix}$, changes from positive to negative with increasing temperature, *i.e.*, ΔH_{mix} and ΔS_{mix} are positive to some extent. The positive ΔH_{mix} can be ascribed to the incompatibility of PNIPAm with ILs owing to strong hydrogen bonding between the amide moiety of NIPAm segments at low temperatures, and the

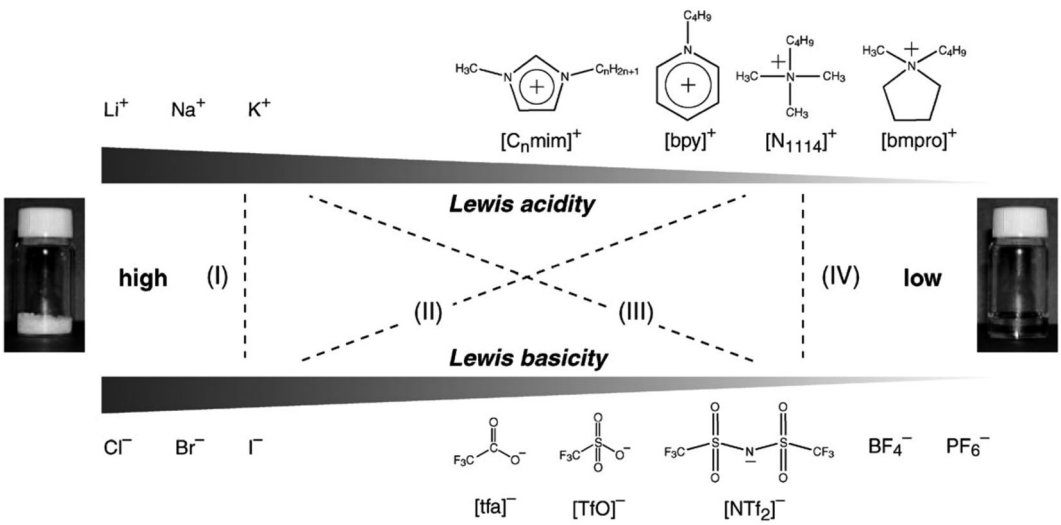

Fig. 3 Salts composed of various combinations of cations and anions, arranged in order of Lewis acidity for cations and Lewis basicity for anions. $[C_n\text{mim}]^+$: 1-alkyl-3-methylimidazolium; $[\text{bpy}]^+$: *N*-butylpyridinium; $[\text{bmpro}]^+$: *N*-butyl-*N*-methylpyrrolidinium; $[\text{N1114}]^+$: trimethylbutylammonium; $[\text{tfa}]^-$: trifluoroacetate; $[\text{TfO}]^-$: trifluoromethanesulfonate; $[NTf_2]^-$: bis(trifluoromethanesulfonyl)imide. Reproduced with permission from ref. 39. The Royal Society of Chemistry 2010.

positive ΔS_{mix} can be ascribed to the increase in the degree of freedom of arrangement caused by mixing the polymer and the solvent.[53] The UCST-type dissolution with an increase of temperature is, thus, ascribed to an increase in the entropic term. In contrast, poly(benzyl methacrylate) (PBnMA) and its derivatives exhibit LCST-type phase separation in [$C_n$mim][NTf_2]

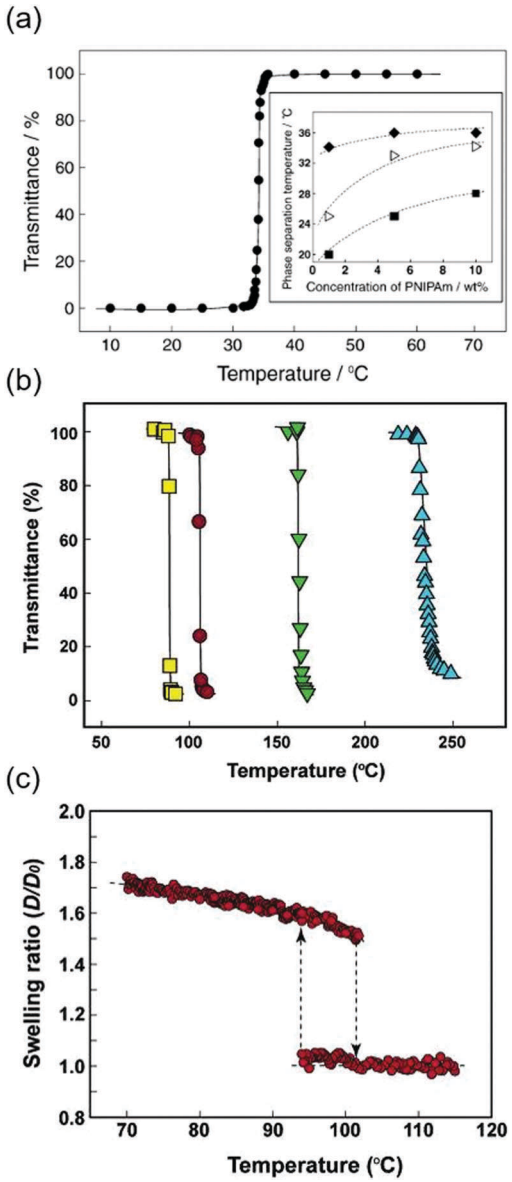

Fig. 4 (a) Temperature dependence of the transmittance at 500 nm for 1 wt% poly(*N*-isopropylacrylamide) (PNIPAm) in [C_2mim][NTf_2]. The inset shows the polymer concentration and degree of polymerization dependencies of the UCST (diamonds, triangles, and squares correspond to 52.3, 38.9, and 15.4 kDa, respectively). Reproduced with permission from ref. 56. The Chemical Society of Japan 2006. (b) Temperature dependence of the transmittance at 500 nm for 3 wt% poly(benzyl methacrylate) (PBnMA) in [$C_n$mim][NTf_2]; yellow squares: [C_1mim][NTf_2]; red circles: [C_2mim][NTf_2]; green inverted triangles: [C_4mim][NTf_2]; blue triangles: [C_6mim][NTf_2]. (c) Equilibrium swelling ratio of a PBnMA gel particle as a function of temperature. The swelling ratio was normalized by the diameter of the gel at 100 °C. Reproduced with permission from ref. 57. American Chemical Society 2007.

(Fig. 4b).[57,58] The LCST-type phase separation results from negative ΔH_{mix} and ΔS_{mix}, indicating that strong interactions between the polymer and the solvent result in both a large stabilization of mixing energy and a loss of mixing entropy owing to the restricted conformations. This phenomenon has been investigated using X-ray scattering and molecular dynamics (MD) simulations, which revealed that structure-forming solvation between the aromatic ring of PBnMA and the imidazolium cation ([$C_n$mim]) leads to a negative entropic mixing term, resulting in LCST-type phase separation.[59,60] PEO also exhibits LCST-type phase separation in [$C_n$mim]BF_4.[61] Moreover, we reported that the mixture of poly(ethyl glycidyl ether) (PEGE) and [C_2mim][NTf_2] exhibits LCST-type phase behavior, even though PEO is soluble in [C_2mim][NTf_2] over a wide temperature range.[62,63] In that study, we evaluated the effect of IL structure on phase behavior and reported that the presence of a methyl substituent at the C-2 position of the imidazolium cation (*i.e.*, 1-alkyl-2,3-dimethylimidazolium) significantly decreases the LCST. That is, in polyether systems, hydrogen bonding between the acidic C-2 proton within the imidazolium cation ([$C_n$mim]) and O atoms within the polyether chains causes structure-forming solvation, resulting in LCST behavior. These thermoresponsive changes in the solubility can introduce other functionalities to soft materials. For example, by chemically crosslinking PBnMA chains, gel particles can be prepared while maintaining the thermoresponsive behavior of PBnMA in ILs (Fig. 4c). The gel particles exhibit a volume phase transition, resulting in reversible changes in the size and swelling ratio with changes in temperature. An azobenzene-containing PBnMA polymer gel has also been reported to show not only thermosensitive volume changes, but also photoresponsive ones.[64] These unique properties of the solution, including the inherent solvent properties of ILs, can widen the potential applications of soft materials comprising BCPs and ILs. Therefore, in this review, we discuss the characteristics of soft materials formed by the self-assembly of BCPs in ILs and their applications.

3. Self-assembly of BCPs in ILs at low polymer concentrations

3.1. Micellization of BCPs in ILs

As discussed in the introduction, BCPs in dilute solution form micelles with various morphologies. Lodge and co-workers first reported that PB-*b*-PEO shows micellization in a typical imidazolium-based IL, [C_4mim]PF_6, at 1 wt% polymer concentration.[65] [C_4mim]PF_6 acts as a good solvent for PEO but a poor solvent for PB, resulting in the formation of micelles with PB cores surrounded by PEO coronas. Fig. 5a–c show microstructures of the micelles formed in ILs, as observed by cryo-TEM. At high volume fractions of PEO blocks, $f_{PEO} > 0.45$, PB-*b*-PEO forms spherical micelles, with the size strongly depending on the polymer chain length (Fig. 5a). On increasing f_{PEO}, other morphologies (cylindrical micelles and vesicles) appear in the solution (Fig. 5b and c). This behavior is

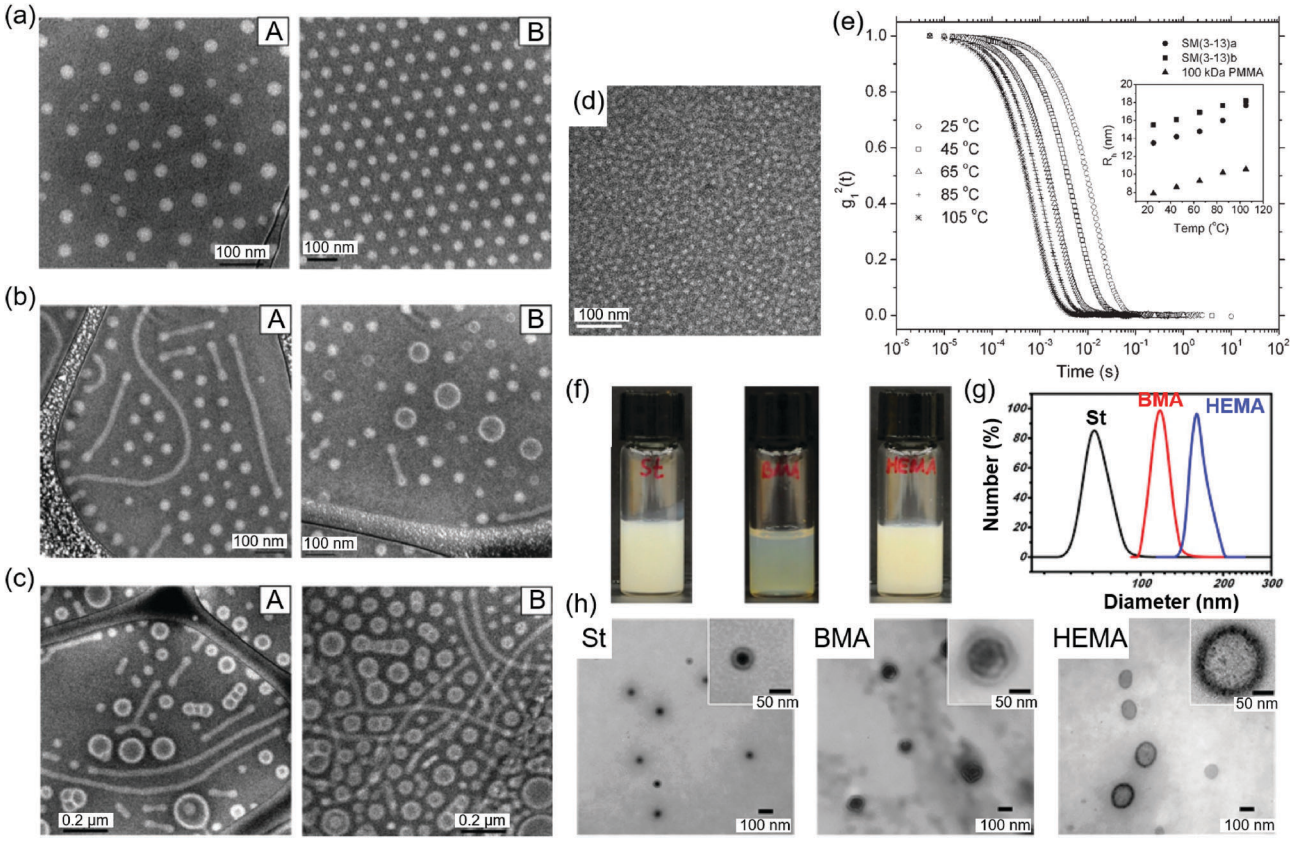

Fig. 5 Cryo-TEM images of 1 wt% poly(1,2-butadiene)-*b*-poly(ethylene oxide) (PB-*b*-PEO) in $[C_4mim]PF_6$ (the PB micellar cores are visualized as a bright color): (a) (panel A) PB-*b*-PEO: 9–20 kDa (f_{PEO} = 0.64); (panel B) PB-*b*-PEO: 9–10 kDa (f_{PEO} = 0.45). (b) PB-*b*-PEO: 9–7 kDa (f_{PEO} = 0.38); (panel A) coexistence of spherical and wormlike micelles; (panel B) coexistence of micelles and vesicles. (c) PB-*b*-PEO: 9–4 kDa (f_{PEO} = 0.25); (panels A and B) coexistence of wormlike micelles and vesicles. Reproduced with permission from ref. 65. American Chemical Society 2006. (d) Cryo-TEM images of 1 wt% polystyrene-*b*-poly(methyl methacrylate), SM(3–13) (PS: 3 kDa; PMMA: 13 kDa), in $[C_4mim]PF_6$. (e) Temperature dependence of squared electric field correlation functions obtained by dynamic light scattering (DLS) of 1 wt% SM(3–13) solutions. The inset shows hydrodynamic radii (R_h) *versus* temperature for 1 wt% SM(3–13) and the PMMA homopolymer (100 kDa) in $[C_4mim]PF_6$. SM(3–13)b was obtained 28 days after the measurement of SM(3–13)a using the same solution. Reproduced with permission from ref. 66. Wiley 2007. (f) Photographs of the final products from RAFT dispersion polymerization of styrene (St), *n*-butyl methacrylate (BMA), and 2-hydroxypropyl methacrylate (HPMA). (g) Distributions of R_h obtained by DLS of the solutions. (h) TEM images (scale bar: 100 nm, inset: 50 nm) of the solutions. Reproduced with permission from ref. 69. American Chemical Society 2015.

analogous to the BCP/water solution discussed in the introduction, implying that the basic principle governing the microstructure is universal, irrespective of solvent. PS-*b*-poly(methyl methacrylate) (PS-*b*-PMMA) also forms micelles in $[C_4mim]PF_6$ with radii of several tens of nm (Fig. 5d).[66] In that study, the high glass transition temperature (T_g) of the PS blocks and the poor solvent nature of $[C_4mim]PF_6$ for the PS blocks result in frozen and nonergodic PS cores in the micelles. Path-dependent morphology and size in the micelle formation in ILs owing to the unique nonergodicity of BCP micelles is also described.[67,68] Fig. 5e shows squared electric field correlation functions obtained by dynamic light scattering (DLS) at various temperatures. The hydrodynamic radius (R_h) linearly increases with increasing temperature, analogous to the behavior of the PMMA homopolymer, indicating swelling of the PMMA coronas. Further, no size transition was observed in this temperature range (25–105 °C), which is below the T_g of the PS blocks. That is, assembly/disassembly of the PS blocks was not induced by the temperature sweep owing to the frozen PS core. After 28 days, almost the same core size was observed owing to the high stability of the micelles and the solvent (IL). ILs can be used as solvents for RAFT polymerization; thus, BCPs can be prepared in ILs by *in situ* polymerization from a macroinitiator. Zhang and Zhu polymerized styrene (St), *n*-butyl methacrylate (BMA), and 2-hydroxypropyl methacrylate (HPMA) from a PEO macroinitiator functionalized with a chain transfer agent (CTA) in $[C_4mim]PF_6$ to obtain PEO-*b*-PSt, PEO-*b*-PBMA, and PEO-*b*-PHPMA suspensions in $[C_4mim]PF_6$ (Fig. 5f).[69] These BCPs exhibited spontaneous microphase-separation to form vesicles. The obtained vesicles were relatively monodisperse, as confirmed by DLS (Fig. 5g) and TEM (Fig. 5h).

3.2. Stimuli-responsiveness of BCP micelles in ILs

The combination of BCP self-assembly and stimuli-responsive polymers in ILs allows control over the morphologies of soft materials using external stimuli. Ueki, Lodge, Watanabe, and co-workers reported reversible assembly/disassembly of BCP micelles in ILs controlled by thermal stimuli for various

combinations of polymers and ILs.[70–73] Fig. 6a shows the concept of doubly thermoresponsive self-assembly of BCPs in ILs.[70] As mentioned in the previous section, PNIPAm and PBnMA exhibit UCST-type and LCST-type phase separation, respectively. If appropriate control of the UCST and LCST of the polymers can be achieved, diblock copolymers comprising PBnMA and PNIPAm blocks in ILs will undergo demicellization induced by the disassembly of the PNIPAm block from the core at an upper critical micelle temperature (UCMT), followed by micellization induced by assembly of the PBnMA block in the core upon heating through a lower critical micellization temperature (LCMT). Fig. 6b shows the normalized intensity and R_h obtained by DLS measurements for PBnMA-*b*-P(NIPAm-*r*-AAm) in [C_2mim][NTf_2] at various temperatures. With increasing temperature, a stepwise sudden decrease and increase in the intensity and size occur, indicating that this BCP exhibits doubly thermoresponsive micellization/demicellization. As the thermoresponsive micellization/demicellization behavior is based on a change in polymer solubility in the IL, this system can be applied to extraction between two solvent phases.[74–76] Fig. 6c shows the concept for a PNIPAm-*b*-PEO micelle shuttle. PNIPAm shows an LCST in water and a UCST in imidazolium-based ILs, leading to the PNIPAm cores assembling in water and disassembling in the IL with increasing temperature. In contrast, the PEO corona block exhibits LCST-type phase separation in water, providing the driving force for micelle transfer from the aqueous to the IL phase according to the change in micelle solubility with increasing temperature. As a result, stepwise micellization in water, transfer of the micelles from the aqueous to the IL phase, and demicellization in the IL were observed. Ueki and co-workers converted the solubility change of the polymer to shrinkage and swelling of a gel by chemically crosslinking the PNIPAm cores of the PNIPAm-*b*-PEO micelle, forming a nanogel.[75] In this system, an increase in temperature induced transfer of the nanogel from the aqueous to the IL phase, and a thermoresponsive change in the radius of the gel was simultaneously observed by DLS. As a micelle shuttle application, Lodge and co-workers demonstrated the transfer of a hydrophobic dye. PB-PEO vesicles containing a hydrophobic dye can be reversibly transferred from the aqueous to the IL phase by sweeping the temperature.[76] These unique behaviors of micelles containing thermoresponsive polymers can contribute to the versatile extraction of target molecules from water to ILs.

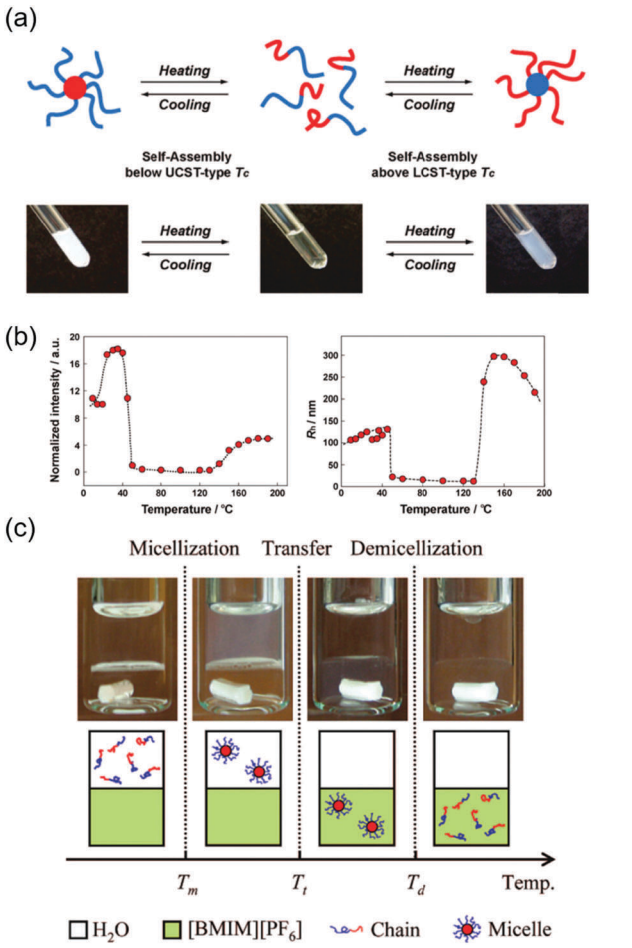

Fig. 6 (a) Concept and photographs of the doubly thermoresponsive self-assembly of a BCP, poly(benzyl methacrylate)-*b*-poly(*N*-isopropylacrylamide-*r*-acrylamide) (PBnMA-*b*-P(NIPAm-*r*-AAm)) in [C_2mim][NTf_2]. The red and blue blocks correspond to UCST-type and LCST-type thermoresponsive blocks, respectively. (b) Thermoresponsive change in the normalized intensity and hydrodynamic radius, R_h, for 1 wt% PBnMA-*b*-P(NIPAm-*r*-AAm) in [C_2mim][NTf_2], obtained by DLS measurements. Reproduced with permission from ref. 70. American Chemical Society 2009. (c) Photographs and concept of a thermoreversible micelle shuttle of PNIPAm-*b*-PEO between water (upper phase) and [C_4mim]PF_6 (lower phase). Reproduced with permission from ref. 74. American Chemical Society 2008.

4. Self-assembly of BCPs in ILs at high polymer concentrations

4.1. Ion gels based on BCP self-assembly

Solidification of ILs while maintaining their unique characteristics, such as high ionic conductivity, is desirable for a variety of device applications. We reported chemically crosslinked polymer gels swollen with ILs (named as ion gels) for the first time by *in situ* polymerization of vinyl monomers in ILs.[77,78] Further, the self-assembly of BCPs has also been utilized to fabricate physically crosslinked ion gels. In particular, ABA-type triblock copolymers composed of an IL-phobic A endblock and an IL-philic B midblock were intensively investigated as a versatile route to fabricate ion gels.[79] At a modest polymer concentration, three-dimensional polymer networks can be formed from micellar aggregates of IL-phobic A blocks as a physical crosslinking point and solvated B blocks as a bridge of micellar aggregates. The first report on ABA triblock-copolymer-based ion gels was by Lodge *et al.*, who selected PS as the A block and PEO as the B block.[80] The triblock copolymer PS-*b*-PEO-*b*-PS (denoted as SOS) dissolved in [C_4mim]PF_6 exhibited a frequency-independent storage modulus (G') at a polymer concentration of 10 wt%, indicative of a gel state (Fig. 7a). Importantly, the polymer network did not have a large influence

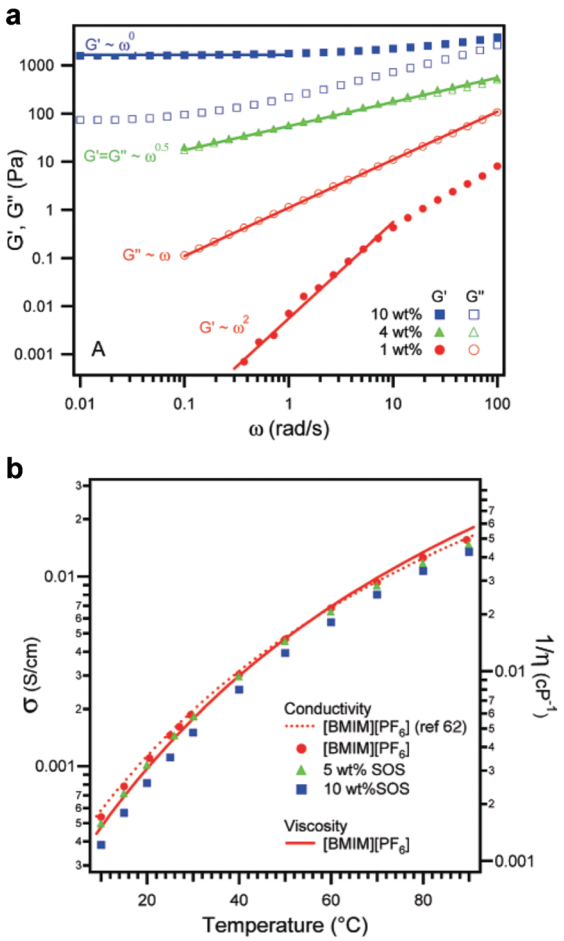

Fig. 7 (a) Frequency sweep measurements for SOS/[C_4mim]PF_6 solutions with various polymer concentrations. (b) Temperature dependence of the ionic conductivity of SOS/[C_4mim]PF_6 ion gels and neat [C_4mim]PF_6. Reproduced with permission from ref. 80. American Chemical Society 2007.

on the ionic conductivity (Fig. 7b). The ion gel retained a high ionic conductivity of greater than 1 mS cm^{-1}, making the ABA triblock-copolymer-based ion gel a promising alternative candidate to conventional polymer electrolytes. PMMA can also be utilized as an IL-philic B block, and the physical properties of the PS-*b*-PMMA-*b*-PS (denoted as SMS) based ion gel were compared with those of the SOS-based ion gel.[81] Although the hydrophobic nature of PMMA is more favorable for electrochemical devices than the hygroscopic nature of PEO, the SMS ion gel had a lower ionic conductivity than the SOS ion gel owing to the high glass transition temperature (T_g) of PMMA (~100 °C), which may somewhat interfere with ionic motions. More recently, hydrophobic poly(ethyl acrylate) with a low T_g (approximately −24 °C) was chosen as a B midblock, resulting in much better balance between elasticity and ionic conductivity than when PMMA was used as the midblock.[82]

4.2. Thermally reversible ion gels

When thermoresponsive polymers in ILs are used as the A blocks of ABA triblock copolymers, temperature-induced sol–gel transitions can be realized. Lodge *et al.* reported UCST-type sol–gel transitions of PNIPAm-*b*-PEO-*b*-PNIPAm (NON) triblock copolymers in [C_2mim][NTf_2].[83] At low temperatures, as PNIPAm endblocks are incompatible with the IL, they aggregate to form micellar cores. As a result, at concentrations higher than the polymer overlapping concentration, the IL-philic PEO midblock bridges the aggregated PNIPAm micelle core, leading to a physically crosslinked ion gel. By increasing the temperature above the UCST-type phase transition temperature of the A block, the A block becomes compatible with the IL, resulting in a gel-to-sol transition upon heating (Fig. 8a). In contrast, by utilizing PBnMA, which undergoes an LCST-type phase transition in ILs, as the A block, PBnMA-*b*-PMMA-*b*-PBnMA (BMB) triblock copolymers in [C_2mim][NTf_2] show temperature-responsive sol–gel transitions with low-temperature sol and high-temperature gel states (Fig. 8b).[84] Owing to the excellent reversibility of the sol–gel transition, temperature-responsive ion gels are promising candidates for thermally processable polymer gel electrolytes. Noro *et al.* reported a different class of thermoreversible ion gels based on ABA triblock copolymers by utilizing supramolecular interactions such as hydrogen bonding[85,86] and metal–ligand interactions.[87] From a practical viewpoint, control of the sol–gel transition temperature (T_{gel}) is of great importance. Tuning of T_{gel} was achieved by introducing IL-phobic PS blocks into the NON triblock copolymer, producing the PNIPAm-*b*-PS-*b*-PEO-*b*-PS-*b*-PNIPAm (NSOSN) pentablock copolymer.[88] By changing the molecular weight of the PS block, T_{gel} can be modulated over a wide temperature range (Fig. 8c). In addition to the polymer architecture, the IL structure itself also significantly influences both the LCST and UCST phase transition temperatures.[54] The T_{gel} of poly(2-phenylethyl methacrylate)-*b*-PMMA-*b*-poly(2-phenylethyl methacrylate) (PPhEtMA-*b*-PMMA-*b*-PPhEtMA, denoted as PMP) in the IL mixture of [C_2mim][NTf_2] and [C_4mim][NTf_2] was easily tuned only by changing the mixing ratio of ILs.[89] Despite these advantages, as ABA triblock-copolymer-based gels inevitably contain loop chains that do not contribute to the network elasticity, the polymer concentration necessary for gelation is higher than that required for an ideal polymer network structure. To achieve more efficient micellar network formation, the ABC architecture containing a solvatophobic C block was found to form hydrogels and ion gels at much lower polymer concentrations than the ABA architecture because of the inhibition of loops back to the same micelle core.[90,91] Furthermore, by utilizing two thermoresponsive polymers, PBnMA and PPhEtMA, with different LCSTs as A and C blocks, the ABC triblock copolymer underwent a hierarchical sol–gel transition *via* stepwise self-assembly of the A and C blocks (Fig. 8d).[92]

4.3. Photocontrol of the sol–gel transition of BCP-based ion gels

Photoresponsiveness can be imparted by incorporating photochromic groups into thermoresponsive polymers. Random copolymers of 4-phenylazophenyl methacrylate (AzoMA) with BnMA (P(AzoMA-*r*-BnMA))[64] and NIPAm (P(AzoMA-*r*-NIPAm)),[93]

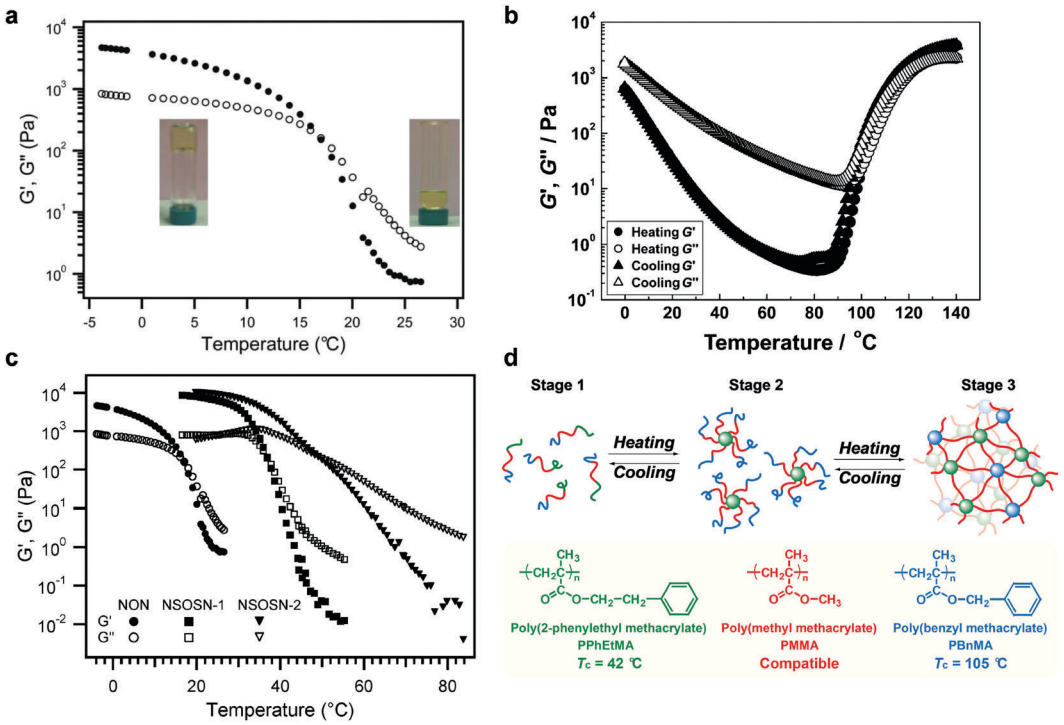

Fig. 8 (a–c) Temperature sweep measurements for (a) 10 wt% NON triblock copolymer, (b) 20 wt% BMB triblock copolymer, and (c) 10 wt% NON triblock and NSOSN pentablock copolymers in $[C_2mim][NTf_2]$. (d) Schematic illustration of the hierarchical sol–gel transition of the PBnMA-*b*-PMMA-*b*-PPhEtMA triblock copolymer in ILs. Reproduced with permission from: (a) ref. 83. Royal Society of Chemistry 2007; (b) ref. 84. Royal Society of Chemistry 2012; (c) ref. 88. American Chemical Society 2008; (d) ref. 92. American Chemical Society 2016.

which show photoinduced phase transitions in ILs, were synthesized by our group. As *cis*-azobenzene has a higher dipole moment than *trans*-azobenzene, the interaction strength between the polymers and the ILs differs depending on the isomerization state of the azobenzene moieties. Consequently, the phase-separation temperatures of P(AzoMA-*r*-BnMA) and P(AzoMA-*r*-NIPAm) in ILs were modulated *via* light irradiation conditions. To achieve photocontrol of the sol–gel transition, a photo-/thermoresponsive triblock copolymer, P(AzoMA-*r*-NIPAm)-*b*-PEO-*b*-P(AzoMA-*r*-NIPAm), was prepared (Fig. 9a).[94] Temperature sweep measurements of the triblock copolymer in an IL demonstrated that the T_{gel} under UV light (*cis*-T_{gel}) is lower than that under visible light (*trans*-T_{gel}). Therefore, at intermediate temperatures between *cis*-T_{gel} and *trans*-T_{gel}, reversible photoinduced sol–gel transitions can be realized by switching light sources (Fig. 9b). Furthermore, photohealing of the ion gel was realized by locally irradiating the damaged area with UV and visible light in a sequential manner.[95] Stress–strain tests for the pristine and healed ion gels revealed that the efficiency of photohealing was as high as 80% (Fig. 9c). However, as the present system required a long time to complete the photohealing process (~64 h), ascribed to the insignificant difference in the relaxation times of the *cis*-ion gel and *trans*-ion gel, widening this difference is of great importance to facilitate a rapid photohealing process.[96] Recently, the photodimerization reaction of coumarin moieties was also exploited to fabricate a photocurable ion gel that can be converted from a thermoresponsive, physically crosslinked ion gel to a thermoirresponsive, chemically crosslinked ion gel *via* UV light irradiation.[97]

As a different approach to realize photocontrolled phase transitions for thermoresponsive polymers in ILs, we recently introduced an azobenzene moiety into an IL structure (Azo-IL).[98] Remarkably, despite the polymer structures not containing photochromic units, the phase transition temperatures of PBnMA and PPhEtMA in ILs containing a small amount of Azo-IL changed with light irradiation, indicating that Azo-IL acted as a photoswitch to modulate the interaction strength between the polymers and the ILs. By combining Azo-IL and thermoresponsive PMP triblock copolymers, photoinduced unimer–micelle[99] and sol–gel[100] transitions were demonstrated (Fig. 9d). Cyclic switching of UV and visible light sources enabled reversible sol–gel transitions triggered by photoisomerization of Azo-IL (Fig. 9e). The strategy of using a photoresponsive IL as a molecular switch enables the application a wide choice of thermoresponsive polymers, paving the way toward a new class of photoresponsive ion gels.

4.4. Microphase-separated structures observed in concentrated BCP solutions in ILs

In high-concentration BCP solutions, long-range-ordered microstructures can be observed, similar to those found in BCP melts.[32] The seminal work by Lodge *et al.* investigated lyotropic mesophases of polybutadiene-*b*-PEO diblock copolymers in ILs using small angle X-ray scattering (SAXS) measurements.[101] Depending on the block ratios and polymer concentrations,

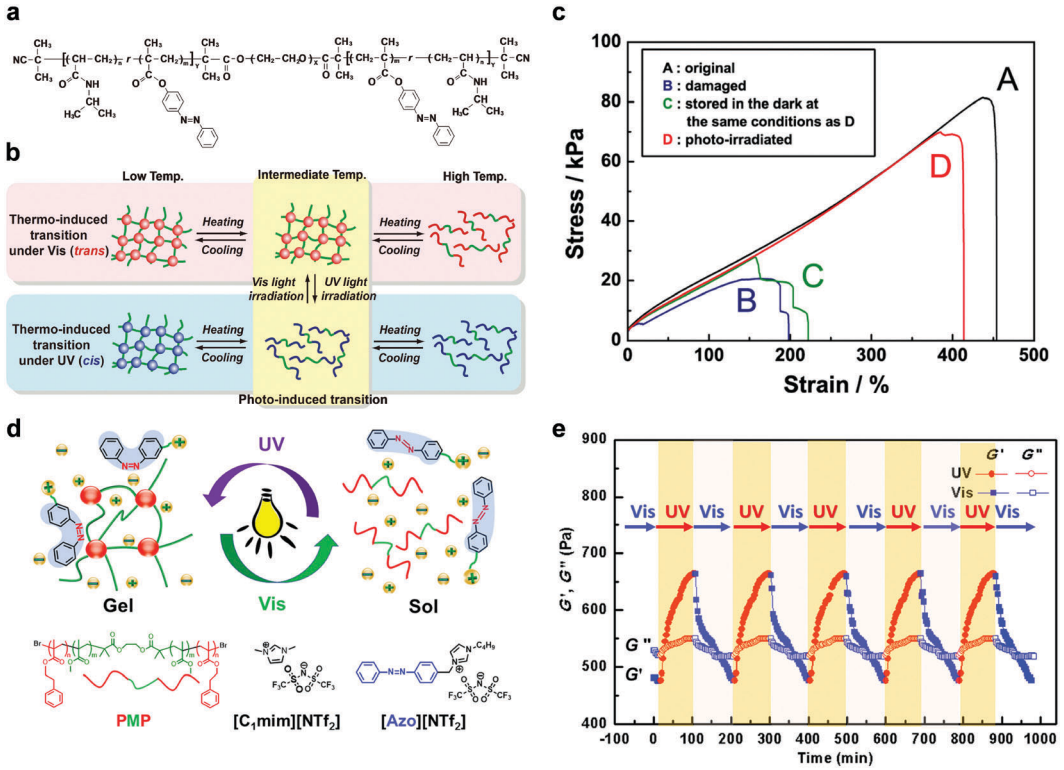

Fig. 9 (a) Chemical structure of the P(AzoMA-*r*-NIPAm)-*b*-PEO-*b*-P(AzoMA-*r*-NIPAm) triblock copolymer. (b) Conceptual illustration of the photo-induced sol–gel transition. Reproduced with permission from ref. 94. Wiley 2015. (c) Tensile stress–strain curves for (A) original, (B) damaged, (C) stored without photohealing, and (D) photohealed ion gels (20 wt%). Reproduced with permission from ref. 95. American Chemical Society 2015. (d) Schematic illustration and chemical structures of polymers and ILs for the photoinduced sol–gel transition triggered by isomerization of Azo-IL as a molecular switch. (e) Reversible sol–gel transition of the PMP triblock copolymer (30 wt%) in the IL mixture of $[C_1mim][NTf_2]$ and $[Azo][NTf_2]$ induced by cyclic irradiation of UV and visible light. Reproduced with permission from ref. 100. Wiley 2018.

several microstructures, including lamellae, hexagonally packed cylinders, and body-centered cubic lattices, were observed (Fig. 10a). Up to now, lyotropic phase behavior in ILs has been investigated for PS-*b*-PEO,[102] PS-*b*-poly(2-vinylpyridine),[103–105] and PS-*b*-PMMA[106] diblock copolymers. More recently, Blakey *et al.* closely investigated the lyotropic phase behavior of the PS-*b*-PMMA diblock copolymer in $[C_2mim][NTf_2]$.[107] The effective Flory–Huggins parameter (χ_{eff}) can be calculated from the order–disorder transition of low-molecular-weight PS-*b*-PMMA samples induced by the addition of an IL, allowing construction of an experimental phase diagram of the effective volume fraction of PS (f_{PS}') against $\chi_{eff}N$ (where N is the effective degree of polymerization) for PS-*b*-PMMA in $[C_2mim][NTf_2]$ (Fig. 10b).

The effect of the microstructures of the BCP/IL composites on the ion transport properties is of great interest. Park *et al.* investigated the relationship between the microphase-separated structures of acid-bearing BCP/IL composites and ionic conductivity.[108–111] The microstructures of poly(styrenephosphonate)-*b*-polymethylbutylene (PSP-*b*-PMB) diblock copolymers upon addition of ILs were investigated using SAXS measurements, which revealed self-assembly of the diblock copolymers into hexagonally packed cylinders (HEX), body-centered cubic lattices (BCC), and A15 lattices with *Pm*3*n* symmetry phases.[111] Two samples with the same diblock copolymer/IL composition but different thermal histories exhibited different morphologies of A15 and HEX phases. Despite the samples having the same BCP/IL composition, the sample with the A15 phase exhibited much higher ionic conductivity than that with the HEX phase (Fig. 11a). This result suggests that the A15 phase with 3D symmetry provides a more efficient ion-conducting pathway than the HEX phase with 2D symmetry (Fig. 11b).

5. Applications of BCP self-assembly in ILs

5.1. Electric double layer transistors

High ionic conductivity and electrochemical stability make ILs promising candidates as gate dielectric materials for electric double layer transistors (EDLTs).[112,113] With high-density carrier accumulation at the IL/semiconductor interface, IL-gated EDLTs can achieve fast switching with relatively low voltage operation (<1 V). For practical application as devices, however, a solid form is more favorable for gate dielectric materials. In this context, ion gels based on BCP self-assembly in ILs have attracted considerable attention. The first example of an ion-gel-gated EDLT was demonstrated by Frisbie *et al.*, who used an ion gel based on self-assembly of the SOS triblock copolymer in

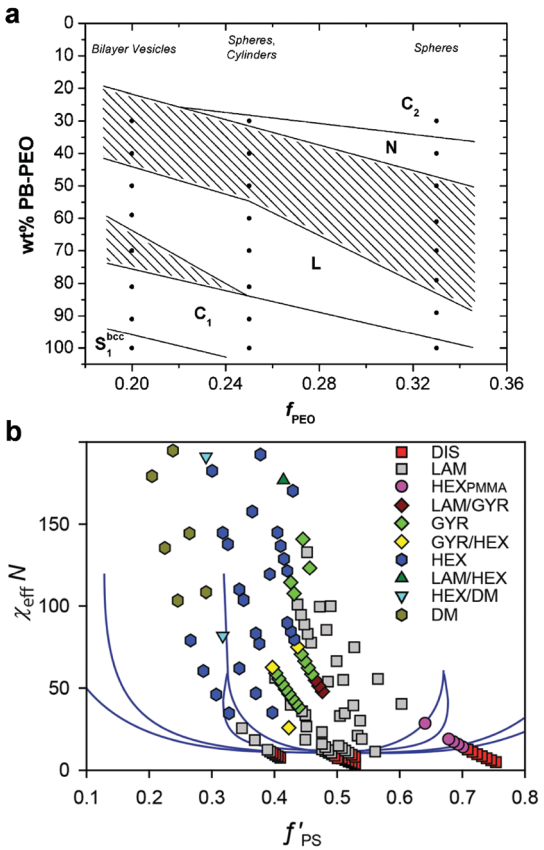

Fig. 10 (a) Lyotropic phase map for PB-*b*-PEO diblock copolymers in $[C_2mim][NTf_2]$. Reproduced with permission from ref. 101. American Chemical Society 2008. (b) Experimental phase diagram for the PS-*b*-PMMA diblock copolymers in $[C_2mim][NTf_2]$ composites. Solid lines represent the theoretical phase diagram for diblock copolymer melts.[7] Reproduced with permission from ref. 107. American Chemical Society 2016.

$[C_4mim]PF_6$ as the gate dielectric material.[114] The gate capacitance of the ion gel reached 41 μF cm^{-2} at 10 Hz and 2.4 μF cm^{-2} at 1 kHz, which were much higher than those of conventional dielectric materials such as SiO_2. In addition, the polarization response time of the ion-gel-gated EDLT is about 1 ms, much faster than those of conventional solid polymer electrolytes (Fig. 12a). Further improvements in gate capacitance at high frequencies and fast polarization response times can be achieved by using $[C_2mim][NTf_2]$-based ion gels (Fig. 12b). This improve behavior is attributed to the SOS/$[C_2mim][NTf_2]$ ion gel having higher ionic conductivity than the SOS/$[C_4mim]PF_6$ ion gel.[115] Importantly, because of the physically crosslinked nature, BCP-based ion gels are solution processable, enabling the cost-effective fabrication of thin-film transistors through aerosol jet printing,[116] spin coating,[117] and transfer printing.[118] Nevertheless, it is still challenging to fabricate flat, thin ion gel films. Therefore, ion gels should be directly fabricated on the semiconductor, restricting the use of semiconductor materials to those that are resistant to the organic solvents used as cosolvents for ion gel printing. To overcome this problem, Iwasa, Takenobu *et al.* first reported organic single-crystal EDLTs using very flat ion gel films.[119] By optimizing the molecular weight of the SMS triblock copolymer, the selection of organic solvent, and the spin-coating conditions, molecularly flat ion gel films were obtained (Fig. 12c), on which single crystals of pentacene, rubrene, and α,ω-bis(biphenyl-4-yl)terthiophene (BP3T) were laminated. When ion gel films are combined with flexible semiconducting films, flexible thin film transistors can be realized.[120] Chemical-vapor-deposition-grown molybdenum disulfide (MoS_2) thin films were transferred onto a flexible polyimide substrate, and subsequently, SMS/$[C_2mim][NTf_2]$ ion gels dissolved in ethyl propionate were cast onto the substrate. The fabricated EDLT showed high flexibility and no electrochemical degradation was observed under bending conditions (Fig. 12d).

5.2. Lithium-ion batteries

The typical liquid electrolytes used in lithium-ion batteries (LIBs) consist of polar organic solvents with dissolved lithium salts. Although liquid electrolytes exhibit high ionic conductivity and low interfacial resistance, the flammability of organic solvents causes LIBs to have serious safety concerns. In this

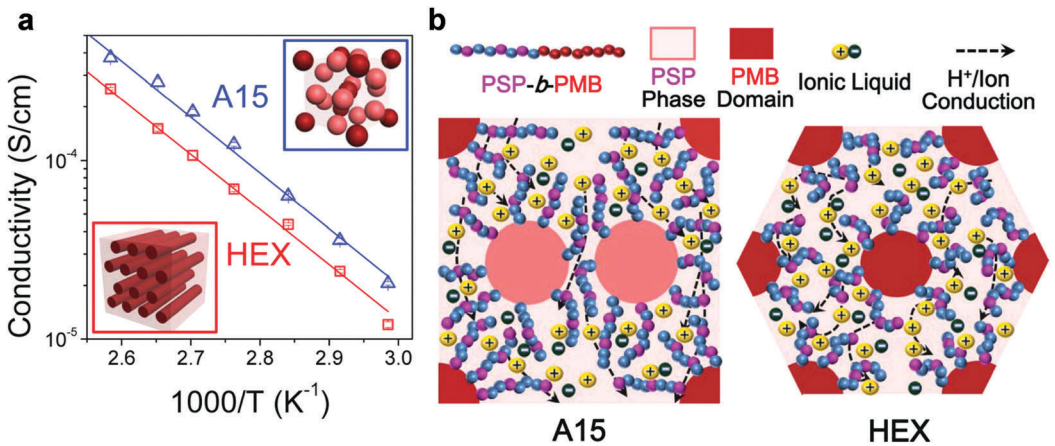

Fig. 11 (a) Ionic conductivity of IL-containing PSP-*b*-PMB diblock copolymers with two different morphologies. (b) Schematic illustrations of the ion-conducting pathways in the A15 and HEX phases. Reproduced with permission from ref. 111. Wiley 2016.

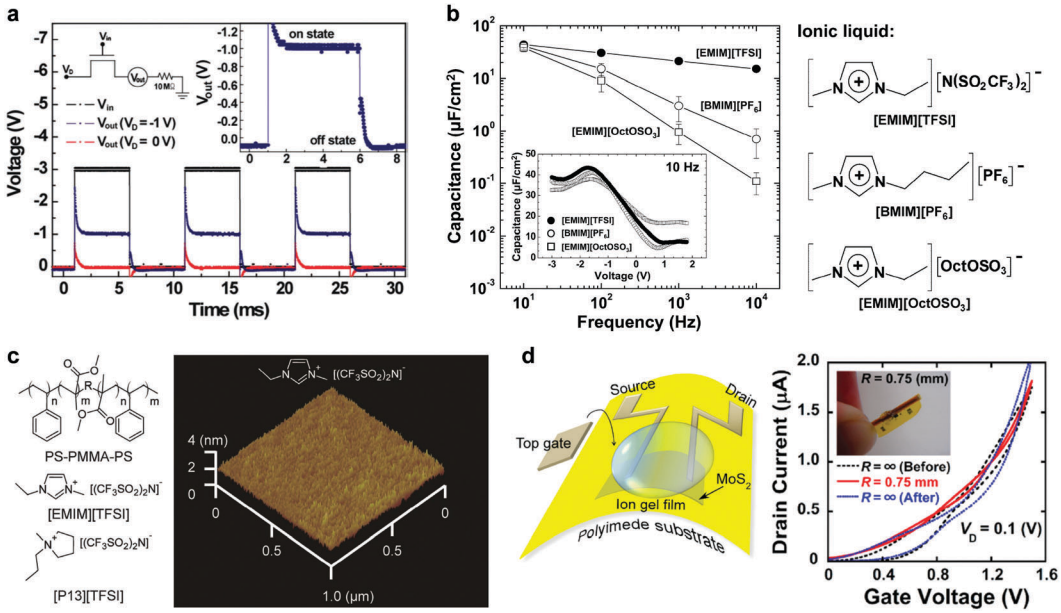

Fig. 12 (a) Transient response of the SOS/[C_4mim]PF_6 ion-gel-gated EDLT. The gate voltage was pulsed at 100 Hz. Reproduced with permission from ref. 114. American Chemical Society 2007. (b) Frequency dependence of the capacitance for SOS ion gels with different ILs. Reproduced with permission from ref. 115. Wiley 2008. (c) (left) Chemical structures of the SMS triblock copolymer and ILs. (right) Atomic force microscopic image of the flat, thin SMS/[C_2mim][NTf_2] ion gel film. Reproduced with permission from ref. 119. Wiley 2012. (d) (left) Schematic illustration of the ion-gel-gated flexible MoS_2 EDLT. (right) Transfer characteristics before bending (black), under bending (red), and after bending (blue). Reproduced with permission from ref. 120. American Chemical Society 2012.

regard, ILs are very attractive as alternatives to organic solvents owing to their nonflammability. However, dissolving lithium salts in ILs induces a significant decrease in ionic conductivity owing to high viscosity.[121] In addition, the lithium transference number (t_{Li}) of the electrolytes is very low,[122–124] which would cause severe concentration gradients in the electrolytes during cell operation. To address these issues, we found that an equimolar mixture of glymes (oligoethers) and lithium salts formed room-temperature liquid complexes, classified as a solvate ionic liquid (SIL).[41,125,126] Remarkably, [Li(glyme)$_1$][NTf_2] showed high ionic conductivity ($\sim$1 mS cm^{-1}), high t_{Li} ($\sim$0.6), and excellent oxidative stability. Leakage of electrolytes is another critical problem in liquid-electrolyte-based LIBs; thus, polymers such as poly(vinylidene fluoride-*co*-hexafluoropropylene) (PVdF-HFP) are used for gelation of Li-containing organic solvents in some commercially available LIBs. We found that, similar to typical ILs, the SMS triblock copolymer can also be utilized to gelate [Li(G4)][NTf_2] (G4: tetraglyme).[127] Above a polymer concentration of 6 wt%, SMS formed transparent gels in [Li(G4)][NTf_2] (Fig. 13a). At a polymer concentration of 30 wt%, SAXS measurements indicated that SMS self-assembled into the BCC phase in [Li(G4)][NTf_2]. Using thermogravimetric analysis, Raman spectroscopy, and pulsed-field gradient spin-echo NMR spectroscopy, stable complex formation of $[Li(G4)]^+$, even in the polymer matrix, was confirmed. The application of [Li(glyme)$_1$][NTf_2]-based ion gels for LIBs was also investigated with three different triblock copolymers: SMS, SOS, and PS-*b*-poly(*n*-butyl acrylate)-*b*-PS (PS-*b*-PBA-*b*-PS, denoted as SBS).[128] Attributed to ligand exchange of Li cations among G4 and PEO chains, the SOS/[Li(G4)][NTf_2] ion gel generated free glymes that did not coordinate Li cations. As a result, the SOS/[Li(G4)][NTf_2] ion gel showed worse thermal stability, poorer oxidation stability, and a lower t_{Li} than the SMS/[Li(G4)][NTf_2] ion gel, resulting in poor charge–discharge cycling stability. This result implies that the absence of free glymes in the electrolyte was crucial for efficient battery performance. Furthermore, the SBS/[Li(G3)][NTf_2] ion gel electrolyte, containing a PBA middle block with a lower T_g and lower affinity for Li cations than PMMA, showed higher ionic conductivity than the SMS/[Li(G4)][NTf_2] ion gel (Fig. 13b). Consequently, the rate performance of the SBS/[Li(G3)][NTf_2] ion gel surpassed that of the SMS/[Li(G4)][NTf_2] ion gel (Fig. 13c). These results indicate that the selection of the B middle block has a significant effect on battery performance. In addition, replacement of the nonionic PS endblock with a poly(lithium acrylate-*r*-acrylic acid) ionomer block improved the mechanical strength of the ion gel electrolyte while maintaining the electrochemical properties owing to the formation of strong physical crosslinks.[129]

5.3. Soft actuators

Electroactive polymer (EAP) actuators are electroresponsive materials that exhibit size or shape changes under voltage application. Typically, EAP actuators can be classified into two categories: electronic EAPs and ionic EAPs.[130,131] Electronic EAP actuators are driven by coulombic attraction between the electrodes, causing a compressive force (Maxwell force) on the insulating elastomers. Electronic EAP actuators show rapid responses, relatively large actuation forces, and can be operated for a long time under ambient conditions. However, a high voltage ($>$1 kV) is required for the actuation of electronic EAP actuators. In contrast, ionic EAP actuators, driven by ion migration and diffusion, can be operated at very low voltage

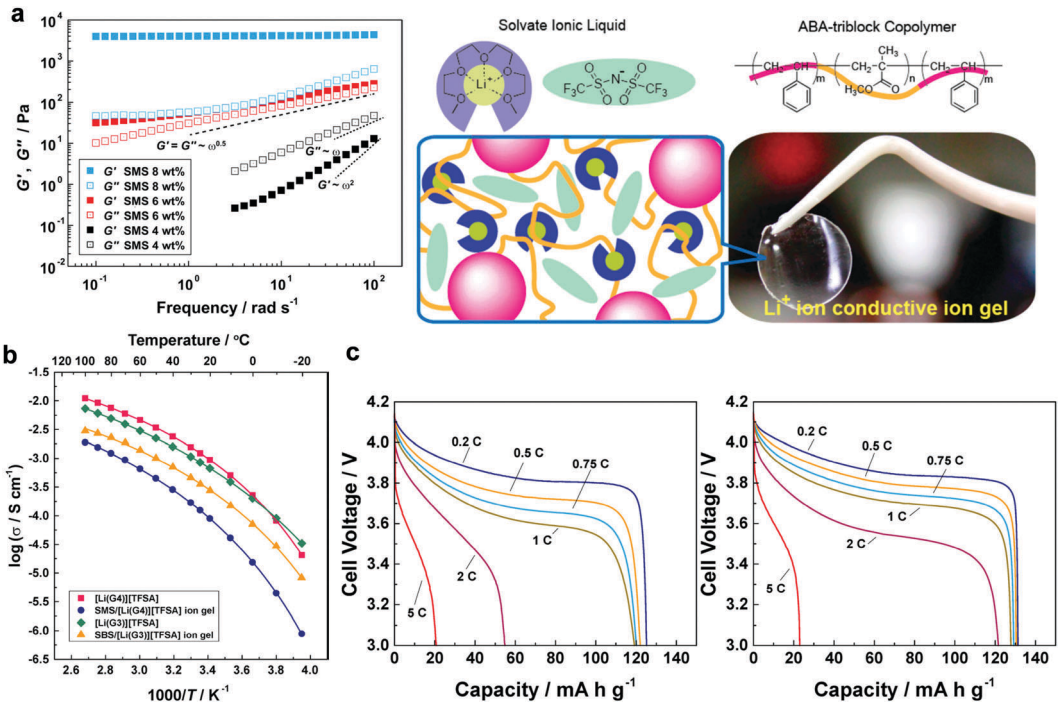

Fig. 13 (a) (left) Frequency dependence of the storage (G') and loss (G'') moduli for different concentrations of SMS in [Li(G4)][NTf_2]. (right) Chemical structures and appearance of the SMS/[Li(G4)][NTf_2] ion gel. Reproduced with permission from ref. 127. American Chemical Society 2014. (b) Temperature dependence of the ionic conductivity for [Li(G4)][NTf_2], 30 wt% SMS/[Li(G4)][NTf_2], [Li(G3)][NTf_2], and 30 wt% SBS/[Li(G3)][NTf_2] electrolytes. (c) Discharge curves for [Li metal anode|ion gel|$LiCoO_2$ composite cathode] cells measured at 60 °C with different C rates. (left) 30 wt% SMS/[Li(G4)][NTf_2]. (right) 30 wt% SBS/[Li(G3)][NTf_2]. Reproduced with permission from ref. 128. American Chemical Society 2018.

(1–2 V). Nevertheless, as conventional ionic EAPs include volatile solvents as the media for ion movement, solvent evaporation prevents long-term operation under an open atmosphere. At this point, the use of nonvolatile ILs can solve this problem, and ionic EAP actuators containing ILs could be operated not only under ambient conditions but also under harsher conditions, such as cosmic space. BCP-based ion gels are promising materials for ionic EAP actuators owing to their solution processability, high ionic conductivity, and mechanical integrity. An ionic EAP actuator was fabricated using the SMS/[C_2mim][NTf_2] ion gel as an electrolyte sandwiched by composite carbon electrodes.[132] Under a low voltage of 2 V, bending motions of the rectangular-shaped actuator were realized (Fig. 14a). The mechanism of the bending motion can be explained by volume change of the electrodes owing to the formation of electric double layers under an electric field, which is caused by the differences in transference numbers and ionic volumes between the cations and the anions of ILs.[133] Anionic[134] and zwitterionic[135] ABA triblock copolymers swollen with ILs were also applied as ionic EAP actuators by Long *et al.* A new class of ionic EAP actuators that exhibit large bending motions and fast responses of tens of milliseconds was reported by Park *et al.*[136] The actuators contained single-ion conducting diblock copolymers and zwitterionic molecules (Fig. 14b). The diblock copolymer was composed of a sulfonated polystyrene, having imidazolium counter cation, (PSS) block and a nonionic polymethylbutylene (PMB) block that formed microphase-separated structures. As only cations can move under the electric field, a large change in electrode volume is expected. Furthermore, addition of an imidazolium-type zwitterion (ZImS) significantly improved the ionic conductivity, even though the zwitterion itself did not contribute to the ionic conductivity. This result implies that ZImS offers a polar medium and facilitates ion dissociation and migration of imidazolium cations. Consequently, the actuator comprising the PSS-*b*-PMB diblock copolymer and the ZImS zwitterion showed a significantly large displacement as well as a fast response time (Fig. 14c).

6. Conclusions and perspectives

Unlike in molecular solvents, such as water and organic solvents, when polymers are dissolved in ILs, cation–anion, polymer–cation, and polymer–anion interactions compete with each other. This unique feature complicates BCP self-assembly in ILs, but simultaneously offers abundant nanoscale structures and characteristic physical properties never observed in conventional solvents. IL-containing intelligent soft materials can be fabricated by incorporating thermoresponsive polymers into one block of BCPs, enabling temperature-induced unimer–micelle or sol–gel transitions in ILs. Furthermore, the introduction of photochromic groups into thermoresponsive polymer chains or IL structures imparts photoresponsiveness, which can be exploited to realize photohealable ion gels. In addition to the unique properties of ILs, such as

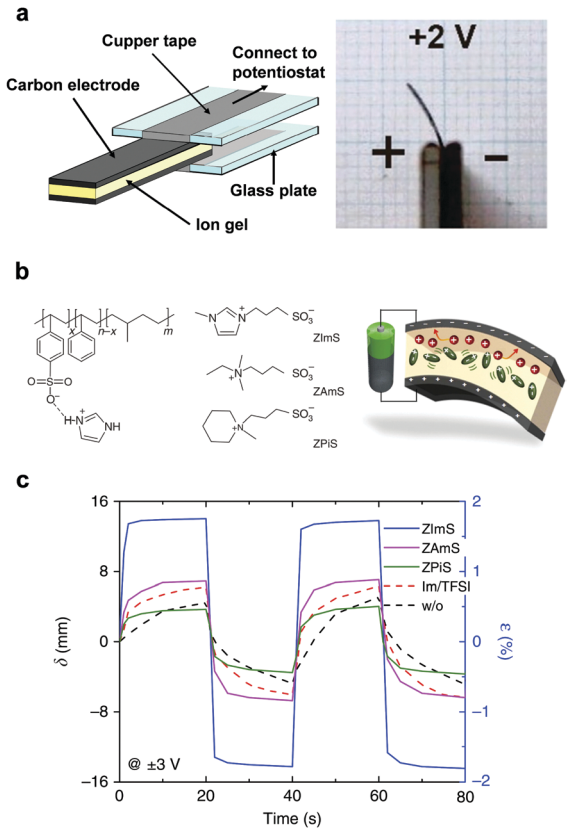

Fig. 14 (a) Schematic illustration of the SMS/[C_2mim][NTf_2] ion gel actuator and a photograph of the bending motion under a voltage of 2 V. Reproduced with permission from ref. 132. American Chemical Society 2012. (b) Chemical structures of the PSS-*b*-PMB diblock copolymer and zwitterions. (c) Displacement and bending strain of the actuators composed of PSS-*b*-PMB and zwitterionic additives. A conventional IL, [C_2mim][NTf_2] (represented as Im/TFSI), was also added for comparison. Reproduced with permission from ref. 136. Nature Publishing Group 2016.

nonflammability, nonvolatility, and thermal stability, physically crosslinked ion gels based on BCP self-assembly in ILs provide mechanical integrity and solution processability, suitable for diverse electrochemical applications such as EDLTs, LIBs, and soft actuators.

The BCP self-assembly in ILs have been widely investigated in the last decade, however, there are still many remaining challenges and future opportunities in this field. The structure–property relationships of the microphase-separated structures of BCPs in ILs and physical properties, such as the mechanical and ion transport characteristics, are not yet fully understood and should be further investigated for fabricating more sophisticated soft materials based on BCP self-assembly in ILs. In this perspective, we concentrated on BCP self-assembly in ILs as solvents, but recently, polymerized IL-based BCPs have also attracted much attention for electrochemical applications.[137–140] Furthermore, utilization of stimuli-responsive BCP-based ion gels to the electrochemical applications would open a new avenue to design novel smart electrochemical devices. For example, thermally responsive ion gels might be exploited to shut down ion conduction at high temperature, significantly improving the safety of electrochemical devices such as lithium secondary batteries.[141,142] In addition to electrochemical applications, biological applications of ILs have been studied in recent years, such as long-term storage of DNA[143] and enzymatic reactions.[144] From this point of view, using self-assembled structures formed by BCPs in ILs as confined media or solidification strategy would be an interesting field that has not been developed yet.

Conflicts of interest

There are no conflicts to declare.

Acknowledgements

This work was financially supported by Grants-in-Aid for Scientific Research (15H05758 to M. W. and 18K14280 to R. T.) and Specially Promoted Research on Iontronics funded by MEXT, Japan. R. T. acknowledges a Research Fellowship awarded by the Japan Society for the Promotion of Science for Young Scientists (17J00756).

References

1 M. Rubinstein and R. H. Colby, *Polymer Physics*, Oxford University Press, New York, 2003.
2 L. Leibler, *Macromolecules*, 1980, **13**, 1602–1617.
3 F. S. Bates and G. H. Fredrickson, *Phys. Today*, 1999, **52**, 32–38.
4 F. S. Bates and G. H. Fredrickson, *Annu. Rev. Phys. Chem.*, 1990, **41**, 525–557.
5 M. W. Matsen and M. Schick, *Phys. Rev. Lett.*, 1994, **72**, 2660–2663.
6 M. W. Matsen and M. Schick, *Macromolecules*, 1994, **27**, 6761–6767.
7 M. W. Matsen and F. S. Bates, *Macromolecules*, 1996, **29**, 1091–1098.
8 A. K. Khandpur, S. Förster, F. S. Bates, I. W. Hamley, A. J. Ryan, W. Bras, K. Almdal and K. Mortensen, *Macromolecules*, 1995, **28**, 8796–8806.
9 D. A. Hajduk, P. E. Harper, S. M. Gruner, C. C. Honeker, G. Kim, E. L. Thomas and L. J. Fetters, *Macromolecules*, 1994, **27**, 4063–4075.
10 D. A. Hajduk, H. Takenouchi, M. A. Hillmyer, F. S. Bates, M. E. Vigild and K. Almdal, *Macromolecules*, 1997, **30**, 3788–3795.
11 M. Kato, M. Kamigaito, M. Sawamoto and T. Higashimura, *Macromolecules*, 1995, **28**, 1721–1723.
12 M. Kamigaito, T. Ando and M. Sawamoto, *Chem. Rev.*, 2001, **101**, 3689–3746.
13 K. Matyjaszewski and J. Xia, *Chem. Rev.*, 2001, **101**, 2921–2990.
14 J.-S. Wang and K. Matyjaszewski, *J. Am. Chem. Soc.*, 1995, **117**, 5614–5615.
15 V. Coessens, T. Pintauer and K. Matyjaszewski, *Prog. Polym. Sci.*, 2001, **26**, 337–377.

16 A. Mühlebach, S. G. Gaynor and K. Matyjaszewski, *Macromolecules*, 1998, **31**, 6046–6052.
17 Y. K. Chong, T. P. T. Le, G. Moad, E. Rizzardo and S. H. Thang, *Macromolecules*, 1999, **32**, 2071–2074.
18 R. T. A. Mayadunne, E. Rizzardo, J. Chiefari, J. Krstina, G. Moad, A. Postma and S. H. Thang, *Macromolecules*, 2000, **33**, 243–245.
19 D. A. Shipp, J.-L. Wang and K. Matyjaszewski, *Macromolecules*, 1998, **31**, 8005–8008.
20 K. A. Davis and K. Matyjaszewski, *Macromolecules*, 2001, **34**, 2101–2107.
21 K. L. Beers, S. G. Gaynor, K. Matyjaszewski, S. S. Sheiko and M. Möller, *Macromolecules*, 1998, **31**, 9413–9415.
22 K. Matyjaszewski, P. J. Miller, J. Pyun, G. Kickelbick and S. Diamanti, *Macromolecules*, 1999, **32**, 6526–6535.
23 S. G. Gaynor, S. Edelman and K. Matyjaszewski, *Macromolecules*, 1996, **29**, 1079–1081.
24 M. W. Matsen and R. B. Thompson, *J. Chem. Phys.*, 1999, **111**, 7139–7146.
25 A. K. Schmitt and M. K. Mahanthappa, *Macromolecules*, 2017, **50**, 6779–6787.
26 F. S. Bates, M. A. Hillmyer, T. P. Lodge, C. M. Bates, K. T. Delaney and G. H. Fredrickson, *Science*, 2012, **336**, 434–440.
27 R. Stadler, C. Auschra, J. Beckmann, U. Krappe, I. Voight-Martin and L. Leibler, *Macromolecules*, 1995, **28**, 3080–3097.
28 W. Zheng and Z.-G. Wang, *Macromolecules*, 1995, **28**, 7215–7223.
29 N. S. Cameron, M. K. Corbierre and A. Eisenberg, *Can. J. Chem.*, 1999, **77**, 1311–1326.
30 L. Zhang and A. Eisenberg, *Science*, 1995, **268**, 1728–1731.
31 A. Choucair and A. Eisenberg, *Eur. Phys. J. E: Soft Matter Biol. Phys.*, 2003, **10**, 37–44.
32 Y. Mai and A. Eisenberg, *Chem. Soc. Rev.*, 2012, **41**, 5969–5985.
33 D. E. Discher and A. Eisenberg, *Science*, 2002, **297**, 967–973.
34 G. Riess, *Prog. Polym. Sci.*, 2003, **28**, 1107–1170.
35 S. Jain and F. S. Bates, *Science*, 2003, **300**, 460–464.
36 T. P. Lodge, B. Pudil and K. J. Hanley, *Macromolecules*, 2002, **35**, 4707–4717.
37 S.-H. Choi, F. S. Bates and T. P. Lodge, *Macromolecules*, 2014, **47**, 7978–7986.
38 A. Blanazs, S. P. Armes and A. J. Ryan, *Macromol. Rapid Commun.*, 2009, **30**, 267–277.
39 K. Ueno, H. Tokuda and M. Watanabe, *Phys. Chem. Chem. Phys.*, 2010, **12**, 1649–1658.
40 W. Xu, E. I. Cooper and C. A. Angell, *J. Phys. Chem. B*, 2003, **107**, 6170–6178.
41 C. A. Angell, Y. Ansari and Z. Zhao, *Faraday Discuss.*, 2012, **154**, 9–27.
42 H. Tokuda, S. Tsuzuki, M. A. B. H. Susan, K. Hayamizu and M. Watanabe, *J. Phys. Chem. B*, 2006, **110**, 19593–19600.
43 M. J. Earle and K. R. Seddon, *Pure Appl. Chem.*, 2000, **72**, 1391–1398.
44 M. Armand, F. Endres, D. R. MacFarlane, H. Ohno and B. Scrosati, *Nat. Mater.*, 2009, **8**, 621–629.
45 M. Watanabe, M. L. Thomas, S. Zhang, K. Ueno, T. Yasuda and K. Dokko, *Chem. Rev.*, 2017, **117**, 7190–7239.
46 S. Zhu, Y. Wu, Q. Chen, Z. Yu, C. Wang, S. Jin, Y. Ding and G. Wu, *Green Chem.*, 2006, **8**, 325–327.
47 Y. Fukaya, K. Hayashi, M. Wada and H. Ohno, *Green Chem.*, 2008, **10**, 44–46.
48 R. P. Swatloski, S. K. Spear, J. D. Holbrey and R. D. Rogers, *J. Am. Chem. Soc.*, 2002, **124**, 4974–4975.
49 U. Kragl, M. Eckstein and N. Kaftzik, *Curr. Opin. Biotechnol.*, 2002, **13**, 565–571.
50 R. Vijayaraghavan, A. Izgorodin, V. Ganesh, M. Surianarayanan and D. R. MacFarlane, *Angew. Chem., Int. Ed.*, 2010, **49**, 1631–1633.
51 T. Welton, *Chem. Rev.*, 1999, **99**, 2071–2084.
52 T. Ueki and M. Watanabe, *Macromolecules*, 2008, **41**, 3739–3749.
53 T. Ueki and M. Watanabe, *Bull. Chem. Soc. Jpn.*, 2012, **85**, 33–50.
54 T. Ueki, *Polym. J.*, 2014, **46**, 646–655.
55 H. G. Schild, *Prog. Polym. Sci.*, 1992, **17**, 163–249.
56 T. Ueki and M. Watanabe, *Chem. Lett.*, 2006, **35**, 964–965.
57 T. Ueki and M. Watanabe, *Langmuir*, 2007, **23**, 988–990.
58 K. Kodama, H. Nanashima, T. Ueki, H. Kokubo and M. Watanabe, *Langmuir*, 2009, **25**, 3820–3824.
59 J. Łachwa, I. Bento, M. T. Duarte, J. N. C. Lopes and L. P. N. Rebelo, *Chem. Commun.*, 2006, 2445–2447.
60 M. Matsugami, K. Fujii, T. Ueki, Y. Kitazawa, Y. Umebayashi, M. Watanabe and M. Shibayama, *Anal. Sci.*, 2013, **29**, 311–314.
61 H.-N. Lee and T. P. Lodge, *J. Phys. Chem. Lett.*, 2010, **1**, 1962–1966.
62 R. Tsuda, K. Kodama, T. Ueki, H. Kokubo, S. Imabayashi and M. Watanabe, *Chem. Commun.*, 2008, 4939–4941.
63 K. Kodama, R. Tsuda, K. Niitsuma, T. Tamura, T. Ueki, H. Kokubo and M. Watanabe, *Polym. J.*, 2011, **43**, 242–248.
64 T. Ueki, A. Yamaguchi, N. Ito, K. Kodama, J. Sakamoto, K. Ueno, H. Kokubo and M. Watanabe, *Langmuir*, 2009, **25**, 8845–8848.
65 Y. He, Z. Li, P. Simone and T. P. Lodge, *J. Am. Chem. Soc.*, 2006, **128**, 2745–2750.
66 P. M. Simone and T. P. Lodge, *Macromol. Chem. Phys.*, 2007, **208**, 339–348.
67 L. Meli and T. P. Lodge, *Macromolecules*, 2009, **42**, 580–583.
68 L. Meli, J. M. Santiago and T. P. Lodge, *Macromolecules*, 2010, **43**, 2018–2027.
69 Q. Zhang and S. Zhu, *ACS Macro Lett.*, 2015, **4**, 755–758.
70 T. Ueki, M. Watanabe and T. P. Lodge, *Macromolecules*, 2009, **42**, 1315–1320.
71 Y. Kobayashi, Y. Kitazawa, T. Komori, K. Ueno, H. Kokubo and M. Watanabe, *Macromol. Rapid Commun.*, 2016, **37**, 1207–1211.
72 H.-N. Lee and T. P. Lodge, *J. Phys. Chem. B*, 2011, **115**, 1971–1977.
73 H.-N. Lee, Z. Bai, N. Newell and T. P. Lodge, *Macromolecules*, 2010, **43**, 9522–9528.
74 Z. Bai, Y. He, N. P. Young and T. P. Lodge, *Macromolecules*, 2008, **41**, 6615–6617.

75 T. Ueki, S. Sawamura, Y. Nakamura, Y. Kitazawa, H. Kokubo and M. Watanabe, *Langmuir*, 2013, **29**, 13661–13665.

76 Z. Bai and T. P. Lodge, *J. Am. Chem. Soc.*, 2010, **132**, 16265–16270.

77 A. Noda and M. Watanabe, *Electrochim. Acta*, 2000, **45**, 1265–1270.

78 M. A. B. H. Susan, T. Kaneko, A. Noda and M. Watanabe, *J. Am. Chem. Soc.*, 2005, **127**, 4976–4983.

79 T. P. Lodge and T. Ueki, *Acc. Chem. Res.*, 2016, **49**, 2107–2114.

80 Y. He, P. G. Boswell, P. Bühlmann and T. P. Lodge, *J. Phys. Chem. B*, 2007, **111**, 4645–4652.

81 S. Zhang, K. H. Lee, C. D. Frisbie and T. P. Lodge, *Macromolecules*, 2011, **44**, 940–949.

82 B. Tang, S. P. White, C. D. Frisbie and T. P. Lodge, *Macromolecules*, 2015, **48**, 4942–4950.

83 Y. He and T. P. Lodge, *Chem. Commun.*, 2007, 2732–2734.

84 Y. Kitazawa, T. Ueki, K. Niitsuma, S. Imaizumi, T. P. Lodge and M. Watanabe, *Soft Matter*, 2012, **8**, 8067–8074.

85 A. Noro, Y. Matsushita and T. P. Lodge, *Macromolecules*, 2008, **41**, 5839–5844.

86 A. Noro, Y. Matsushita and T. P. Lodge, *Macromolecules*, 2009, **42**, 5802–5810.

87 A. Noro, S. Matsushima, X. He, M. Hayashi and Y. Matsushita, *Macromolecules*, 2013, **46**, 8304–8310.

88 Y. He and T. P. Lodge, *Macromolecules*, 2008, **41**, 167–174.

89 Y. Kitazawa, T. Ueki, S. Imaizumi, T. P. Lodge and M. Watanabe, *Chem. Lett.*, 2014, **43**, 204–206.

90 C. Zhou, M. A. Hillmyer and T. P. Lodge, *J. Am. Chem. Soc.*, 2012, **134**, 10365–10368.

91 C. C. Hall, C. Zhou, S. P. O. Danielsen and T. P. Lodge, *Macromolecules*, 2016, **49**, 2298–2306.

92 Y. Kitazawa, T. Ueki, L. D. McIntosh, S. Tamura, K. Niitsuma, S. Imaizumi, T. P. Lodge and M. Watanabe, *Macromolecules*, 2016, **49**, 1414–1423.

93 T. Ueki, Y. Nakamura, A. Yamaguchi, K. Niitsuma, T. P. Lodge and M. Watanabe, *Macromolecules*, 2011, **44**, 6908–6914.

94 T. Ueki, Y. Nakamura, R. Usui, Y. Kitazawa, S. So, T. P. Lodge and M. Watanabe, *Angew. Chem., Int. Ed.*, 2015, **54**, 3018–3022.

95 T. Ueki, R. Usui, Y. Kitazawa, T. P. Lodge and M. Watanabe, *Macromolecules*, 2015, **48**, 5928–5933.

96 X. Ma, R. Usui, Y. Kitazawa, R. Tamate, H. Kokubo and M. Watanabe, *Macromolecules*, 2017, **50**, 6788–6795.

97 R. Tamate, T. Ueki, A. M. Akimoto, R. Yoshida, T. Oyama, H. Kokubo and M. Watanabe, *RSC Adv.*, 2018, **8**, 3418–3422.

98 C. Wang, X. Ma, Y. Kitazawa, Y. Kobayashi, S. Zhang, H. Kokubo and M. Watanabe, *Macromol. Rapid Commun.*, 2016, **37**, 1960–1965.

99 C. Wang, K. Hashimoto, J. Zhang, Y. Kobayashi, H. Kokubo and M. Watanabe, *Macromolecules*, 2017, **50**, 5377–5384.

100 C. Wang, K. Hashimoto, R. Tamate, H. Kokubo and M. Watanabe, *Angew. Chem., Int. Ed.*, 2018, **57**, 227–230.

101 P. M. Simone and T. P. Lodge, *Macromolecules*, 2008, **41**, 1753–1759.

102 P. M. Simone and T. P. Lodge, *ACS Appl. Mater. Interfaces*, 2009, **1**, 2812–2820.

103 J. M. Virgili, A. Hexemer, J. A. Pople, N. P. Balsara and R. A. Segalman, *Macromolecules*, 2009, **42**, 4604–4613.

104 J. M. Virgili, M. L. Hoarfrost and R. A. Segalman, *Macromolecules*, 2010, **43**, 5417–5423.

105 J. M. Virgili, A. J. Nedoma, R. A. Segalman and N. P. Balsara, *Macromolecules*, 2010, **43**, 3750–3756.

106 L. Gwee, J.-H. Choi, K. I. Winey and Y. A. Elabd, *Polymer*, 2010, **51**, 5516–5524.

107 T. M. Bennett, K. S. Jack, K. J. Thurecht and I. Blakey, *Macromolecules*, 2016, **49**, 205–214.

108 S. Y. Kim, S. Kim and M. J. Park, *Nat. Commun.*, 2010, **1**, 1–7.

109 H. Y. Jung, S. Y. Kim, O. Kim and M. J. Park, *Macromolecules*, 2015, **48**, 6142–6152.

110 O. Kim, S. Y. Kim, J. Lee and M. J. Park, *Chem. Mater.*, 2016, **28**, 318–325.

111 H. Y. Jung, O. Kim and M. J. Park, *Macromol. Rapid Commun.*, 2016, **37**, 1116–1123.

112 R. Misra, M. McCarthy and A. F. Hebard, *Appl. Phys. Lett.*, 2007, **90**, 052905.

113 S. Ono, S. Seki, R. Hirahara, Y. Tominari and J. Takeya, *Appl. Phys. Lett.*, 2008, **92**, 103313.

114 J. Lee, M. J. Panzer, Y. He, T. P. Lodge and C. D. Frisbie, *J. Am. Chem. Soc.*, 2007, **129**, 4532–4533.

115 J. H. Cho, J. Lee, Y. He, B. S. Kim, T. P. Lodge and C. D. Frisbie, *Adv. Mater.*, 2008, **20**, 686–690.

116 J. H. Cho, J. Lee, Y. Xia, B. Kim, Y. He, M. J. Renn, T. P. Lodge and C. D. Frisbie, *Nat. Mater.*, 2008, **7**, 900–906.

117 K. H. Lee, S. Zhang, T. P. Lodge and C. D. Frisbie, *J. Phys. Chem. B*, 2011, **115**, 3315–3321.

118 K. H. Lee, S. Zhang, Y. Gu, T. P. Lodge and C. D. Frisbie, *ACS Appl. Mater. Interfaces*, 2013, **5**, 9522–9527.

119 Y. Yomogida, J. Pu, H. Shimotani, S. Ono, S. Hotta, Y. Iwasa and T. Takenobu, *Adv. Mater.*, 2012, **24**, 4392–4397.

120 J. Pu, Y. Yomogida, K.-K. Liu, L.-J. Li, Y. Iwasa and T. Takenobu, *Nano Lett.*, 2012, **12**, 4013–4017.

121 B. Garcia, S. Lavallée, G. Perron, C. Michot and M. Armand, *Electrochim. Acta*, 2004, **49**, 4583–4588.

122 Y. Saito, T. Umecky, J. Niwa, T. Sakai and S. Maeda, *J. Phys. Chem. B*, 2007, **111**, 11794–11802.

123 T. Frömling, M. Kunze, M. Schönhoff, J. Sundermeyer and B. Roling, *J. Phys. Chem. B*, 2008, **112**, 12985–12990.

124 J.-W. Park, K. Yoshida, N. Tachikawa, K. Dokko and M. Watanabe, *J. Power Sources*, 2011, **196**, 2264–2268.

125 K. Yoshida, M. Nakamura, Y. Kazue, N. Tachikawa, S. Tsuzuki, S. Seki, K. Dokko and M. Watanabe, *J. Am. Chem. Soc.*, 2011, **133**, 13121–13129.

126 K. Ueno, K. Yoshida, M. Tsuchiya, N. Tachikawa, K. Dokko and M. Watanabe, *J. Phys. Chem. B*, 2012, **116**, 11323–11331.

127 Y. Kitazawa, K. Iwata, S. Imaizumi, H. Ahn, S. Y. Kim, K. Ueno, M. J. Park and M. Watanabe, *Macromolecules*, 2014, **47**, 6009–6016.

128 Y. Kitazawa, K. Iwata, R. Kido, S. Imaizumi, S. Tsuzuki, W. Shinoda, K. Ueno, T. Mandai, H. Kokubo, K. Dokko and M. Watanabe, *Chem. Mater.*, 2018, **30**, 252–261.

129 T. Kawazoe, K. Hashimoto, Y. Kitazawa, H. Kokubo and M. Watanabe, *Electrochim. Acta*, 2017, **235**, 287–294.

130 S. Hara, T. Zama, W. Takashima and K. Kaneto, *Polym. J.*, 2004, **36**, 151–161.

131 A. O'Halloran, F. O'Malley and P. McHugh, *J. Appl. Phys.*, 2008, **104**, 071101.

132 S. Imaizumi, H. Kokubo and M. Watanabe, *Macromolecules*, 2012, **45**, 401–409.

133 S. Imaizumi, Y. Kato, H. Kokubo and M. Watanabe, *J. Phys. Chem. B*, 2012, **116**, 5080–5089.

134 E. Margaretta, G. B. Fahs, D. L. Inglefield, C. Jangu, D. Wang, J. R. Heflin, R. B. Moore and T. E. Long, *ACS Appl. Mater. Interfaces*, 2016, **8**, 1280–1288.

135 T. Wu, D. Wang, M. Zhang, J. R. Heflin, R. B. Moore and T. E. Long, *ACS Appl. Mater. Interfaces*, 2012, **4**, 6552–6559.

136 O. Kim, H. Kim, U. H. Choi and M. J. Park, *Nat. Commun.*, 2016, **7**, 13576.

137 W. Qian, J. Texter and F. Yan, *Chem. Soc. Rev.*, 2017, **46**, 1124–1159.

138 M. D. Green, J.-H. Choi, K. I. Winey and T. E. Long, *Macromolecules*, 2012, **45**, 4749–4757.

139 J.-H. Choi, Y. Ye, Y. A. Elabd and K. I. Winey, *Macromolecules*, 2013, **46**, 5290–5300.

140 J. R. Nykaza, Y. Li, Y. A. Elabd and J. Snyder, *J. Electroanal. Chem.*, 2016, **783**, 182–187.

141 Z. Chen, P.-C. Hsu, J. Lopez, Y. Li, J. W. F. To, N. Liu, C. Wang, S. C. Andrews, J. Liu, Y. Cui and Z. Bao, *Nat. Energy*, 2016, **1**, 15009.

142 H. Yang, Z. Liu, B. K. Chandran, J. Deng, J. Yu, D. Qi, W. Li, Y. Tang, C. Zhang and X. Chen, *Adv. Mater.*, 2015, **27**, 5593–5598.

143 R. Vijayaraghavan, A. Izgorodin, V. Ganesh, M. Surianarayanan and D. R. MacFarlane, *Angew. Chem., Int. Ed.*, 2010, **49**, 1631–1633.

144 J. Gorke, F. Srienc and R. Kazlauskas, *Biotechnol. Bioprocess Eng.*, 2010, **15**, 40–53.